Measurement and evaluation of OH-airglow spectra over Svalbard

Master's thesis in meteorology

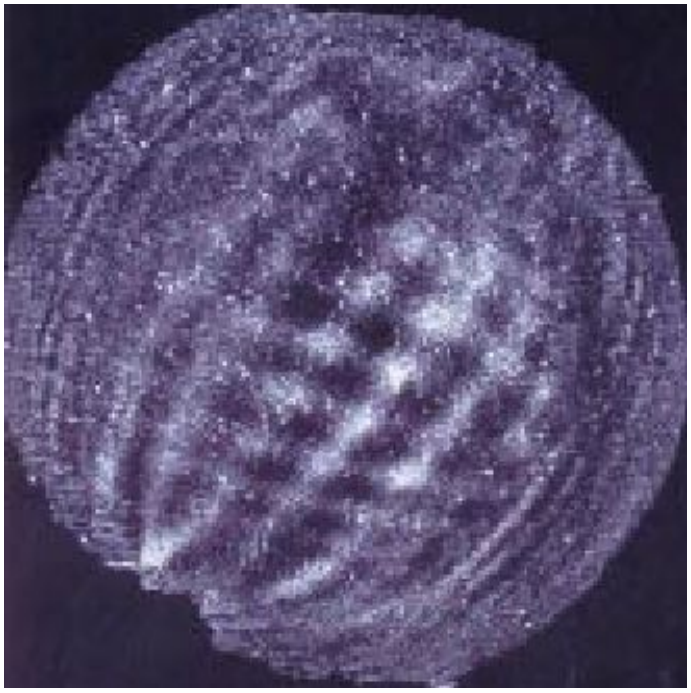

Kristian Pagh Nielsen

Spring 2001

Geofysisk Institutt
Universitetet i Bergen

Contents

1 Introduction

Before the 20^{th} century the atmosphere above 10 kilometers height was considered to have a fairly simple structure. From the laws of gases, the temperature in the atmosphere was thought to decrease linearly with height, until the height at which the mixing time due to diffusion is considerably less than the time required for establishing gravitational separation of the gasses. Above this height that was calculated to be around 100 kilometers, the atmosphere was expected to consist of lighter gases (Mirtov 1961). The temperature profile in the troposphere is in average in good agreement with this. So it was quite surprising that the first measurements from a balloon in, what was named, the stratosphere by Teisserenc de Bort in 1902 indicated that the temperature here was constant with respect to height. In fact it is often referred to as the most surprising event in the history of meteorology. Later it was found that the temperature higher up in the stratosphere increases with height, until the gradient turns once again, and the expected negative gradient is found in the region now defined as the mesosphere. The stratosphere and mesosphere are often combined in the definition "the middle atmosphere".

The explanation of the highly stratified stratosphere is, as it is well known today, the heating that occurs due to ozone molecule absorption of ultraviolet radiation. The presence of these chemically unstable ozone molecules was first explained by Chapman (1930), who by considering a pure oxygen atmosphere could explain that photodissociation of molecular oxygen would produce atomic oxygen that quickly would recombine with an oxygen molecule to produce ozone. From Chapman's theory it could be deduced that the maximum production rate of ozone should be over the equator. However the ozone concentrations observed had minimal values over the equator. This led Dobson (1930) to believe that strong rising motion over the equator and strong sinking motion over the poles drove a stratospheric circulation that transported ozone away from the equator. Later evidence was found for this circulation by Brewer (1949) and it was dubbed the Brewer-Dobson circulation.

Since then other atmospheric molecules and atoms that contribute to the thermal structure of the stratosphere and mesosphere have been found. Thus heating is also caused by molecular oxygen that absorbs ultraviolet radiation in the upper mesosphere (and in the thermosphere) and a slight heating occurs due to stratospheric absorption of long wave radiation by carbondioxide and dinitrogenoxide. Cooling due to emission of long wave radiation from carbondioxide, ozone and to a lesser extent water vapor is also of great importance to the thermal structure (Brasseur & Solomon 1986). On figure 1.1 the vertical absorption pattern of the incoming solar radiation in the atmosphere is shown. As it can be seen almost all radiation with wavelengths less than 300 nm is absorbed before it reaches the surface of the Earth. With the radiation from 0 to 100 nm mainly being absorbed in the thermosphere, the radiation from a 100 nm to 200

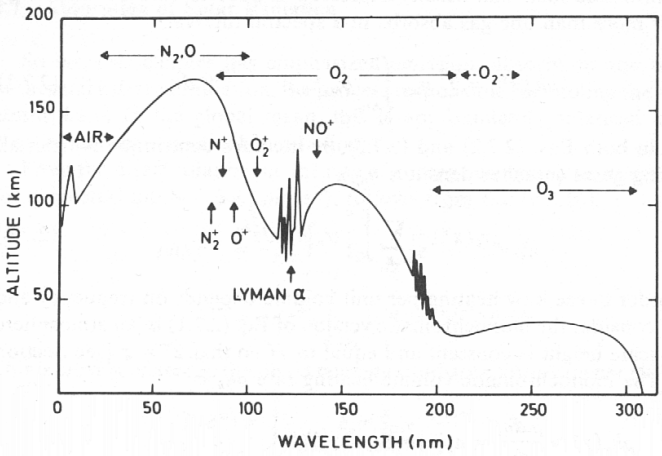

Figure 1.1: *The average heights in the atmosphere at which solar radiation of a certain wavelength is extincted to 1/e of the intensity at the top of the atmosphere. This corresponds to the height of maximum radiative energy deposition. The figure is taken from (Brasseur & Solomon 1986).*

nm mainly in the mesosphere and the radiation between 200 nm and 300 nm mainly in the stratosphere. The main atmospheric species that are responsible for the absorption are marked on the figure, with indication of the wavelength intervals in which they are important (Brasseur & Solomon 1986).

1.1 The middle atmosphere in radiative equilibrium

Fels (1985) calculated the middle atmospheric temperature, from a model in which only the radiative heating and cooling were included. Fels included the chemical species that are responsible for absorption and emission, the cloud distributions and the temperature variations in the troposphere. The result for January shown in figure 1.2 is representative for the average temperature distribution with respect to latitude in January. In figure 1.3 the observed average temperatures in the atmosphere are shown for comparison. Please note that the two figures have the north pole on opposite sides! As it can be seen there is large difference between the atmospheric temperatures in the two figures. The largest differences are seen at the winter pole, where the observed temperatures at 80°N are approximately 100 K higher than the radiatively modeled temperatures in most of the mesosphere. Over the stratospheric winter pole the difference is around 50 K at 30 km height and 40 K at 20 km height. These large departures from the radiative equilibrium show that other influences than radiation are of great importance to the atmospheric thermodynamics.

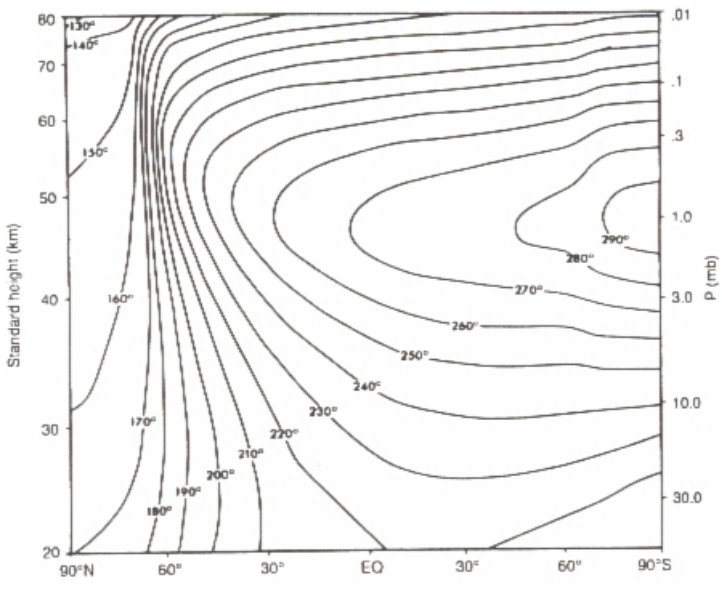

Figure 1.2: *The atmospheric temperature distribution calculated from the assumption of radiative equilibrium by Fels. The figure is taken from (Holton 1992).*

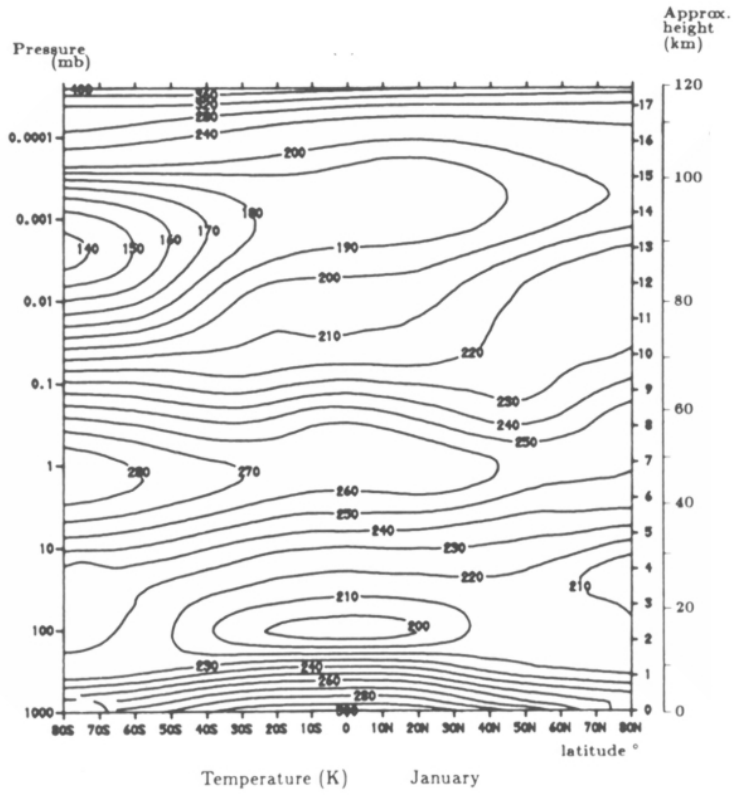

Figure 1.3: *The average observed temperature for January. The figure is taken from (Holton 1992).*

1.2 The effect of the meridional circulation

The Brewer-Dobson circulation in the stratosphere mentioned above causes the departure from radiative equillibrium temperatures in most of the stratosphere. The Brewer-Dobson circulation is part of the atmospheric meridional circulation, which is the global circulation between the equator and the poles averaged with respect to latitude. In regions in which the meridional circulation is upwards air parcels are cooled adiabatically and in regions in which the meridional circulation is downwards air parcels are warmed adiabatically. Therefore the atmospheric temperature in general is different from the temperatures calculated from radiative equillibrium considerations. The large departures over the winter pole in January are however also strongly effected by the dramatic variations in both temperature and circulation that occur during northern hemisphere winter in the stratosphere.

1.3 The effects of planetary waves and gravity waves

These dramatic variations were first described by Scherlag (1952), who reported that the lower and middle stratosphere over central Europe experienced strong warmings of more than 50 K within a few days in wintertime. He named these "Die explosionsartigen Stratosphärenwärmungen des Spätwinters", which has been translated to: "the late wintertime sudden stratospheric warmings". This phenomenon can be explained by the development of planetary waves originating from the troposphere (Matsuno 1971). The planetary scale waves redistribute warmer air from lower latitudes into the polar areas of the stratosphere that is otherwise cold due to the lack of incoming radiation during wintertime. This process will be described briefly in section 2.

Observations show that the frequency and strength of stratospheric warmings differ from year to year in what appears to be a random pattern. It has however been shown that this variability to a high degree can be explained from the long period variations in sea surface temperature anomalies, e. g. the El Niño Southern Oscillation (Blackmon, Geisler & Pitcher 1983) and the quasi-biennual oscillation in the equatorial stratosphere (Dunkerton, Delisi & Baldwin 1988). In the last few years the 11-year oscillation of the equatorial stratosphere also has been shown to have a large effect on the occurrence of stratospheric warmings in the northern hemisphere (Kodera & Yamazaki 1990), (Dunkerton & Baldwin 1992), (Labitzke & van Loon 1997) and (Labitzke & van Loon 1999).

Observations have also been done of planetary waves in the mesosphere e.g. (Pancheva, Lastovicka & de la Morena 1991) and (Nielsen et al. 2001). However the effects of these on the thermodynamics is unknown and it is believed that it is small in comparison to the effect of gravity waves. The geographic distribution of gravity wave drag on the mean flow is believed to be the main reason for the departure from the thermal equilibrium temperatures in the mesosphere (Andrews, Holton & Leovy 1987).

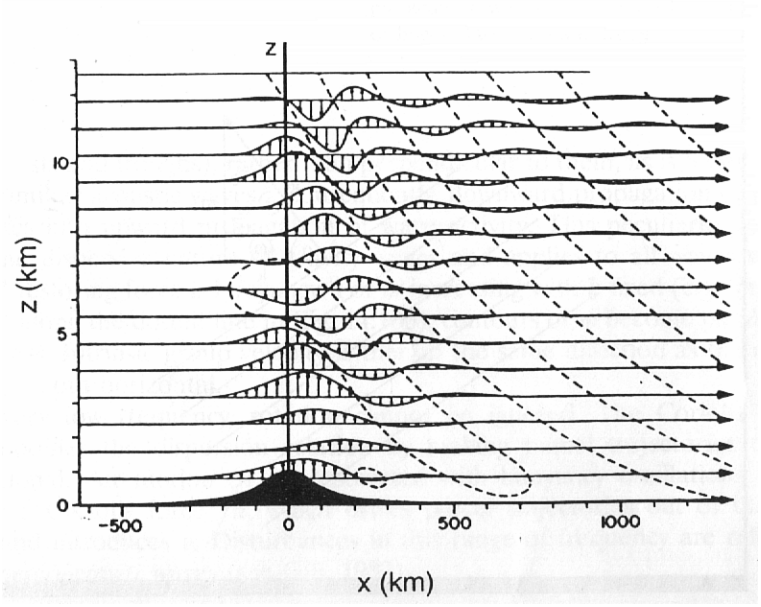

Figure 1.4: *Internal gravity waves in the atmosphere. The horizontal lines are streamlines and the vertical arrows show the vertical component of the wind at a specific point. The black silhouette is a mountain that obstructs the flow. The figure is taken from Salby (1996).*

Hines (1960) was the first to suggest that internal gravity waves can be the explanation for large disturbances on short time scales in the middle atmosphere and the upper atmosphere. Gravity waves in this context being the buoyancy waves that are created when air parcels are displaced from a balance between the pressure gradient- and gravity-forces in a stably stratified environment (see figure 1.4). Indications have later been found that gravity waves do not only cause disturbances on short time scales but in fact supply the major forcing on the general atmospheric circulation that is needed to explain the large difference between the observed mesospheric temperatures (Fig. 1.3) and those calculated from the assumption of radiative equilibrium (Fig. 1.2) (Lindzen 1981), (Holton 1982) and (Holton 1983).

1.4 Problems, methods and main themes of the research of the stratosphere and mesosphere in year 2000

The main problem of the research of the upper stratosphere and mesosphere is that standard weather balloons cannot go very much higher than 30 km up in the atmosphere due to the decrease in air density. Therefore the only way to make in situ measurements of this part of the atmosphere is with rockets that cannot be launched with anything near the coverage in space and time that is obtained with weather balloons in the lower atmosphere. Making it necessary to use various remote sensing methods to get observations of the atmosphere above 30 km height over longer periods.

The importance of the atmosphere above 30 km is emphasized by the fact that ozone molecules mainly absorb radiation above this height as it can be seen in figure 1.1. Ozone molecules, as it is well known, are very sensitive to changes in the surrounding chemical species (Brasseur & Solomon 1986). As mentioned earlier the distribution of these ozone molecules (and other chemical species) are highly dependent on the atmospheric dynamics. Therefore one of the major issues of middle atmospheric research is to gain understanding of the general circulation of these regions of the atmosphere. In particular the effects of gravity waves, which seem to drive a large-scale circulation cell from the mesospheric summer pole to the mesospheric winter pole by causing strong downward motion in the high latitude areas of the winter mesosphere and upward motion in the summer mesosphere, i. e. a secondary circulation above the stratospheric Brewer-Dobson circulation cell (Brasseur & Solomon 1986).

Since the end of the eighties most of the progress in the research of the mesosphere has been done within the scientific community CEDAR (Couplings Energetics and Dynamics in Atmospheric Research). CEDAR was started in 1988 with its main devotion to obtaining increased communication between the group of scientists working with improving the methods of remote sensing that are used to make observations in the middle atmosphere, and the group of scientists working with modeling of the aeronomy (chemistry, dynamics and photochemistry) of the atmosphere. Figure 1.5 shows the global network of ground-based observation sites within the CEDAR community.

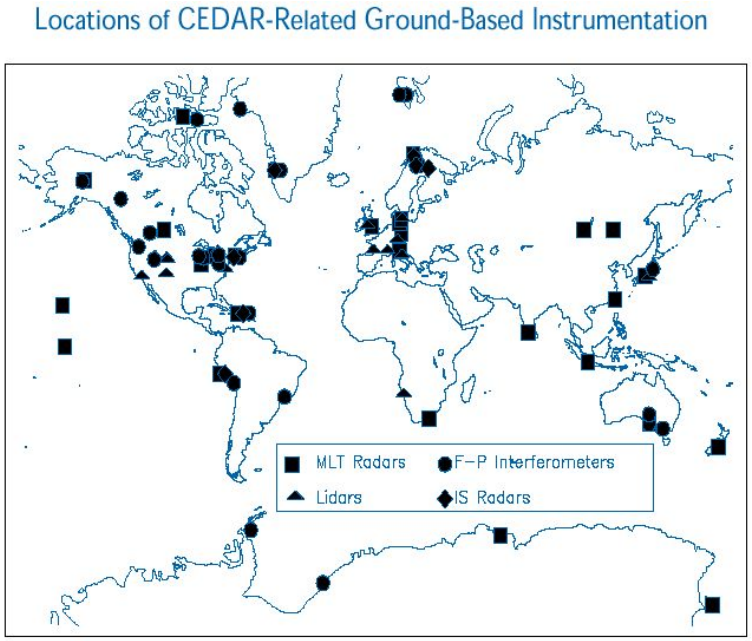

Figure 1.5: *The global distribution of middle and upper atmospheric observatories and RADARs. The figure is taken from the CEDAR phase III-report (1998).*

Below is a listing of the main instruments that are used for observations of the

middle atmosphere.

- **Photometers** With photometers emissions from photochemically exited atoms and molecules can be measured, giving information on the reaction rates of the chemical processes creating them. They are used onboard rockets and satellites, and to gain spatial information from ground based sites with scanning photometers. Photometers have their limitation in that emissions from atmospheric species are so weak that they can only be detected at night. The same limitation applies to spectrometers, imagers and interferometers.

- **Spectrometers/spectrographs** As the photometers, spectrometers and spectrographs measure atom and molecule emissions in the line of sight. But where the photometers can measure only a single wavelength band, the spectrometers and spectrographs can measure a spectral range of emissions. They are used mainly for derivation of rotational temperatures of excited oxygen (that are found around a height of 95 km) and hydroxyl molecules (that are found around a height of 87 km).

- **Imagers** are basically photometers equipped with all-sky lenses and CCD-detectors to image emissions from the whole sky. With the imagers information on the propagation of gravity waves over the sky can be obtained.

- **Interferometers** are also used for measuring the spectrum of atmospheric emissions. The measurements can be used to calculate horizontal winds and temperatures.

- **RADARs** With the RADARs the neutral winds in the 80-100 km region can be measured. In the last years RADARs have also been developed that can be used to determine temperatures from meteor decay-rates. Radars can measure continiously.

- **LIDARs** or Laser-RADARs as they come in two variants. The first is the resonance LIDARs that can measure the resonance of various alkali metals that are found in the 80-110 km region. From these measurements high accuracy profiles of the horizontal winds and temperatures can be calculated. The second is the Rayleigh LIDARs that can measure the atmospheric backscatter from which the temperature and wind can be deduced up to 60 km height. LIDARs can measure only when the sky is clear.

The various methods have various advantages and the combination of as many types of measurements as possible is needed for the best results. For instance a wind measuring interferometer and a temperature measuring spectrometer can be combined with an imager that gived the all-sky structural variations of the emissions that are

investigated. The list of instruments above is mainly taken from the CEDAR phase III-report (1998).

One of four key issues of CEDAR is polar aeronomy. This branch of aeronomy has got increased attention, as many important processes occur in the polar areas:

- The strong winter mesospheric downward motion that is presumably induced by gravity wave drag as illustrated on figure 1.6[1] and the corresponding summer mesospheric upward motion.

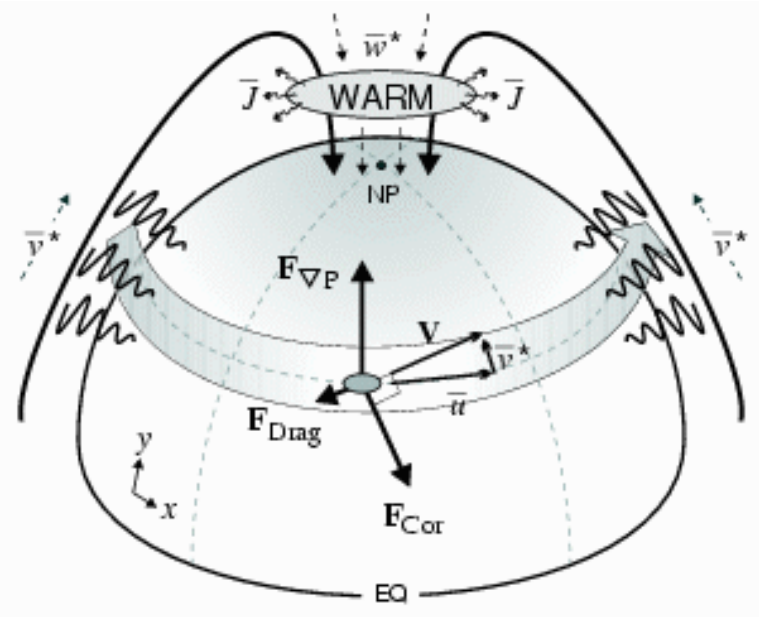

Figure 1.6: *A vector diagram of the gravity wave drag forced downward motion in the winter hemisphere. The figure is taken from (Duck 2000).*

- Proton precipitation events has been observed to cause ozone depletions of 10% in the polar areas(Stephenson & Scourfield 1992).

- Indications that the dynamical features of the polar stratosphere are dynamically coupled to the dynamics in the mesosphere through gravity wave propagation have been found in observations (Myrabø, Deehr & Lybekk 1984), (Lastovicka 1989), (Whiteway & Duck 1996), (Duck, Whiteway & Carswell 1998), (Walterscheid, Sivjee & Roble 2000) and (Nielsen et al. 2001) and models (Holton 1983) and (McLandress & McFarlane 1993).

- Statistical analysis show that the temperature in the summer polar stratosphere follow the variations of the solar cycle (van Loon & Labitzke 1999) and (van Loon

[1]The theory is explained in section 2.4.2

& Shea 2000). However the physical explanation of such a coupling of the solar cycle to the summer stratosphere still remains to be found.

- The effect of the large increase in atmospheric carbondioxide is a main theme of the research of the mesosphere and thermosphere, as the effect of carbondioxide is thought to be much larger in these regions of the atmosphere (CEDAR 1998). Many observations indicate that this is true. There has been a large increase in the sightings of clouds in the upper mesosphere (notilucent clouds) (Gadsden 1998) and the ionospheric radio-signal reflection heights in the upper mesosphere have decended with 20-40 m/year during the last 50 years (Bremer 1997). This is in good agreement with the results from atmospheric models, which have estimated that the carbondioxide increase will cause a temperature trend of approximately -0.2 K/year in average in the mesosphere (e. g. (Berger & Dameris 1993) and (Akmaev & Fomichev 1998)). Some temperature measurements however give different results. Thus temperature measurements in the upper mesosphere made from rockets from the russian island Heisa (81°N, 58°E) show a temperature trend of -0.9 K/year at 75 km height (Golitsyn et al. 1996), opposed to the trend of -0.024 K/year in the polar summer mesosphere deduced by Lübken (2000) from falling sphere measurements during the nineties. In general there is almost no cooling trend during the nineties compared to the the previous decades (Pers. comm. Lastovicka 2000), which is odd considering that the CO_2 increase in that time period probably was the largest in historical time.

1.5 The Svalbard OH-timeseries

Investigation of the polar mesosphere in the northern region has only been performed from a few facilities in the world (fig. 1.5), as the arctic northwards of 70°N has only poor infrastructure. The first ground based measurements of the polar arctic mesosphere were started in the early eighties in connection with the Multi-National Svalbard Auroral Expedition (Deehr et al. 1980). Deehr et al. used an Ebert-Fastie spectrometer to measure the hydroxyl airglow. Since then, measurements of the hydroxyl airglow have been performed almost every winter, making the Svalbard OH-airglow timeseries the longest timeseries of polar mesospheric measurements.

Measurements with the Ebert-Fastie spectrometer of the OH-airglow over Svalbard is evaluated in this thesis. In particular with respect to the dependence on the processes in the atmosphere below.

Meinel (1950) identified the OH emission bands in the near infrared part of the night sky spectrum. From these emissions the neutral temperature in the upper mesosphere can be found by analyzing the distribution of the rotational lines of the individual rotational bands of the OH-spectrum (Kvifte 1959). The theory will be described in section 4.

This method of determining the upper mesospheric temperature has been used to study the airglow temperature over Svalbard. A series of articles on these subjects were published in eighties.

Myrabø, Deehr and Sivjee (1983) found large amplitude variations of both the OH(8-3)-vibrational band intensity and temperature. They were the first to suggest that these variations are actual variations rather than noise, from a comparison with earlier measurements and the fact that similar temperature measurements had a much lower standard deviation at mid-latitudes.

Myrabø (1984) found the temperature variations typically being around ± 20 K in the internal gravity wave period range (minutes to hours) with extremes of ± 70 K within a few hours, indicating that the gravity wave activity in the polar winter atmosphere is more frequent and violent than is the case for lower latitudes. The extreme temperatures of the winter 1982/1983 was found to be 158 K and 298 K. On a larger time scale Myrabø found that the daily mean temperatures show a wave-like pattern with deviations from the mean, each lasting for about 3-10 days. Also a semi-diurnal variation of the temperatures was found with an amplitude of 3 K in December 1982.

Myrabø and Deehr (1984) found no indications of an influence from the geomagnetic activity on the OH(8-3) temperatures from a comparison between the temperatures, the planetary geomagnetic K_p-index and the direction of the interplanetary magnetic field.

Myrabø, Deehr & Lybekk coupled an unusually strong mesospheric cooling at newyears eve 1982 to the stratospheric warming occurring simultaneously (Myrabø et al. 1984).

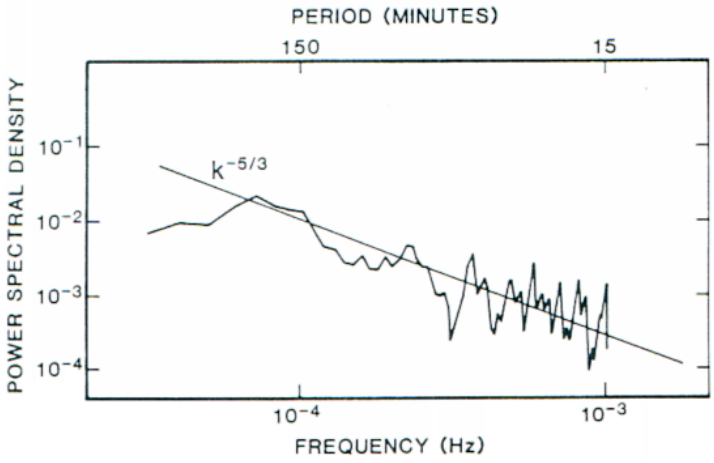

Figure 1.7: *The average spectrum of temperature variations between November 25 and 27, 1983. The figure is taken from (Myrabø et al. 1987).*

Myrabø et al. (1987) by evaluating the OH(8-3) rotational temperatures of November 1983 found evidence for breaking gravity waves in the airglow layer. In a spectral analysis (see figure 1.7) of the temperature variations they found that the power spectral density depended on the frequency in the power -5/3 for the variations with periods between 15 and 150 minutes. This is the same spectral distribution that turbulence in the troposphere displays (Gage 1979). Their measurements implied a vertical eddy diffusion coefficient in the range between $8 \cdot 10^2 - 8 \cdot 10^3$ m^2/s. Since 1987 similar spectra have been observed in many other studies and are today recognized as a global feature of the upper mesosphere (Pers. comm. Lastovicka 2000).

From the winter 1983/1984 and onward it was found that the OH(6-2) vibrational band was better to use than the OH(8-3). The OH(6-2) band has been measured since then.

Myrabø (1986) described the OH-airglow variations over Svalbard in the four winter seasons 1980–1985 (there were no measurements made in the winter of 1981/1982). He found that the monthly averages for November, December, January, February and March were 206 K, 212 K, 223 K, 212 K and 198 K respectively. The maxima of the temperatures occurred in December in some years and in January in others. In this paper another unusually strong mesospheric cooling or "mesocool" is described and questions are asked of why the "mesocools" often occur before the stratospheric warmings and why the mesosphere warms up quickly after the "mesocool", even when the stratospheric warming persists.

Comparison of the Svalbard OH-measurements to similar measurements performed at a lower latitude station (Poker Flat, Alaska) showed that both short period and seasonal temperature variations are consistently larger in the OH-airglow over Svalbard (Pers. comm. Deehr 1999).

Similar measurements of the upper mesosphere over Antarctica indicate a large asymmetry, as clear winter solstice minima are seen in the temperatures there, and smoother temperature variations compared to Svalbard (Pers. comm. Deehr 1999).

The aim of the present thesis work has been to measure and analyze OH-airglow temperatures over Svalbard and assess the influence on these temperatures from stratospheric phenomena. During the investigation it has been found that the best approach to understand the dynamical connection between the stratosphere and mesosphere was to make a detailed analysis of data from the winter 1999/2000.

The respective parts of the thesis are written to be understandable for a bachelor degree student in meteorology or a bachelor student in physics.

2 Dynamical theory

In this section the governing hydrodynamic equations for the polar winter middle atmosphere will be described, followed by a description of the main dynamic features of the middle atmosphere.

2.1 The governing equations of hydrodynamics on a β-plane

The three governing equations are the momentum balance equation (the second law of Newton), the continuity equation and the energy balance equation.

In the middle atmosphere the equations are often written in log-pressure co-ordinates, in which the vertical co-ordinate is defined as

$$z = -Hln\frac{p}{p_s} \tag{2.1}$$

Where p is the pressure, p_s is 1000 hPa and H is the atmospheric scale height (which is around 7 km in average in the middle atmosphere) (Brasseur & Solomon 1986).

The momentum balance equations in log-pressure co-ordinates are

$$\frac{D\vec{v}}{Dt} = -f\vec{k} \times \vec{v} - \nabla\vec{\Phi} + \vec{X} \tag{2.2}$$

$$\frac{\partial\Phi}{\partial z} = \frac{R}{H}T \tag{2.3}$$

Here equation (2.2) is the horizontal momentum balance equation. The variables in this are: $\vec{v}$ the horizontal velocity vector and f the planetary vorticity. Φ is the geopotential height that is defined as the work required to raise a unit mass from mean sea level to a specific height. The terms on the right hand side of the equation are the Coriolis force (the force on an air parcel due to the Earth rotation), the pressure gradient force and the turbulent drag force (Holton 1992).

Equation (2.3) is the vertical momentum balance equation. Here R is the gas constant for dry air and T is the temperature. The equation is also the assumption of hydrostatic equilibrium.

When using these equations in atmospheric science, they should be written in spherical co-ordinates as a function of latitude and longitude, for the highest degree of accuracy. Here however they are written using the cartesian co-ordinates x and y besides the log-pressure co-ordinate, as this is a qualitative description rather than a quantitative description. The x-direction is also called the zonal direction and it is defined as positive towards East. The y-direction is also called the meridional direction and is

defined as positive towards North. Often the governing equations are considered on a β-plane, as is the case here. This is an approximation, in which the planetary vorticity (f) is estimated as a Taylor-development with only the two first terms

$$f \approx f_0 + \beta y,\ f_0 \equiv 2\Omega sin\phi_0,\ \beta \equiv \frac{df_0}{dy} = 2\Omega\frac{cos\phi_0}{a} \tag{2.4}$$

where f is a function of a reference latitude (ϕ_0) and the angular momentum of the Earth (Ω). a is the radius of the Earth (Holton 1992).

The continuity equation is

$$\frac{\partial(\rho_0 u)}{\partial x} + \frac{\partial(\rho_0 v)}{\partial y} + \frac{\partial(\rho_0 w)}{\partial z} = 0 \tag{2.5}$$

The energy balance equation in log-pressure co-ordinates is

$$\frac{DT}{Dt} + (\frac{\kappa T}{H})w = \frac{J}{c_p},\ \kappa = \frac{R}{c_p} \tag{2.6}$$

Here w is the vertical velocity with respect to the log-pressure co-ordinate, J is the rate of heating per unit mass owing to radiation, conduction and latent heat release per unit mass, i. e. the diabatic heating per unit mass, and c_p is the specific heat capacity at constant pressure (Holton 1992).

2.2 The Eulerian mean equations

When explaining the general circulation of the atmosphere it is useful to consider the zonally averaged equations, as they give a good overview over the thermodynamical processes that are important in the atmosphere. However information about the structure in the zonal direction cannot be described with these equations. The zonal average can be applied to the equations if the variables are split into zonal means (shown with overbars) and perturbation values (shown with primes), i. e. $A = \overline{A} + A'$, where A can be any variable. If this is applied to the continuity equation (2.5), the result is

$$\frac{\partial(\rho_0 \overline{v_a})}{\partial y} + \frac{\partial(\rho_0 \overline{w_a})}{\partial z} = 0 \tag{2.7}$$

When the Eulerian mean equations are derived, not only the zonal average, but also the quasi-geostrophic scaling scheme is applied. This is done by splitting the horizontal winds into geostrophic and ageostrophic components and determining the negligible terms in the equations. Thereby it can be found that the advection by ageostrophic

winds and some of the perturbation terms coming from the zonal averaging can be removed from the equations without serious error (Holton 1992). Thus the zonal mean zonal momentum balance equation, the zonal mean meridional momentum balance equation and the zonal mean energy balance equation become

$$\frac{\partial \overline{u_g}}{\partial t} - f_0 \overline{v_a} = -\frac{\partial(\overline{u_g' v_g'})}{\partial y} + \overline{X} \tag{2.8}$$

$$f \overline{u_g} + \frac{\partial \overline{\Phi}}{\partial y} = 0 \tag{2.9}$$

$$\frac{\partial \overline{T}}{\partial t} + \frac{N^2 H}{R} \overline{w_a} = -\frac{\partial(\overline{v_g' T'})}{\partial y} + \frac{\overline{J}}{c_p} \tag{2.10}$$

The subscripts g and a in equations (2.7), (2.8) and (2.9) note geostrophic and ageostrophic wind components respectively. In equation (2.8) the first term on the right side is new. This term is an approximation of the zonal mean convergence of the eddy momentum fluxes per unit mass, as the zonal dimension is averaged out and the vertical eddy flux convergences have been neglected. Eddies are perturbations from the zonal mean that affect the zonal mean circulation. The pressure gradient force term has vanished as this was a derivative in the zonal direction. In equation (2.10) there also is a new term on the right side. This is proportional to the convergence of the meridional heat fluxes (the meridional heat flux = $\rho_0 c_p \overline{T'v'}$). The convergence of eddy momentum flux and the convergence of meridional heat flux represent all the contributions to the Eulerian mean equations due to regional departures from the zonal mean winds and temperatures (Holton 1992).

From equations (2.8) and (2.10) it can be seen that changes in the zonal mean zonal wind and the zonal mean temperature arise from small imbalances between the forcing terms (the convergence of eddy momentum flux, the zonally averaged turbulent drag force, the convergence of eddy heat flux and the diabatic heating) and the mean meridional circulation (the Coriolis force and the adiabatic cooling term) (Holton 1992).

In the middle atmosphere it is a good assumption to make that the diabatic heating is only caused by radiation, as there is almost no water vapor in this part of the atmosphere. Thereby there is no latent heating and the heat conduction is of no importance compared to the other terms of the equation. Due to the fact that the actual temperatures are much larger than the radiative equilibrium temperatures, the diabatic heating can be parameterized as proportional to the difference between the zonal mean temperature and the radiative equilibrium temperature (T_r)

$$\frac{\overline{J}}{c_p} = -\alpha_r[\overline{T} - T_r] \tag{2.11}$$

where α_r is the Newtonian cooling rate. London (1980) made a theoretical calculation of the diabatic heating rate including the ultraviolet absorption of ozone and molecular oxygen, and the cooling through infrared emission from the vibrational relaxation of carbondioxide. The result was that the diabatic heating rate was close to -10 K/day at 80°N in winter between 50 km height and 100 km height (the mesosphere) decreasing to around -1 K/day between 20 km height and 30 km height at the same latitude in winter. From equation (2.11) and the actual temperature deviations in January (described in section 1.1 and figures 1.2 and 1.3) the Newtonian cooling rate can be found. This is thus of the order 0.1 at 80 km height and of the order 0.01 at 30 km height. From these numbers the maximum rate of temperature change due to diabatic cooling can be estimated by substituting equation (2.11) into equation (2.10) and assuming that T_r does not vary significantly with respect to time:

$$\frac{(\overline{T} - T_r)(t)}{(\overline{T} - T_r)(t=0)} = exp(-\alpha_r t) \tag{2.12}$$

This is the solution of equation (2.10) if it is assumed that there is no meridional circulation and no eddy fluxes. With the values at 80 km height put into equation (2.12) the halfing time of the temperature difference is a week, while it is a month when the values at 30 km height are used. This gives an indication of the timescales at which the diabatic term has effect in the middle atmosphere.

The effect of the other forcing terms in the Eulerian mean equation in different heights of the arctic middle atmosphere in winter will be discussed in the following sections. First the effects of the large scale eddies will be discussed and then the effects of the small scale eddies and their propagation will be discussed.

2.3 The effect of large scale eddies on the thermodynamics of the middle atmosphere

The contributions to the Eulerian mean equations that are due to the perturbations from the zonal mean, gravity waves and turbulence are all gathered in the eddy terms that are used in section 2.2. Eddies are in this context not only vortices but also waves or any other dynamical structure that gives contribution to the zonal mean quantities from the perturbation quantities of the atmosphere. To illustrate how for instance waves contribute to the Eulerian mean equations figure 2.1 has been made, this shows an example of the wind and temperature distribution in a planetary scale wave. As it

can be seen the eddy heat flux (defined as $\overline{v'T'}$) is positive in a wave developed from a basic state with the temperature gradient towards South. The eddy momentum flux (defined as $\overline{u'v'}$) is positive provided that the wave has the asymmetry on the figure, with the steep crests in the region where the wind is southward. Had the asymmetry been opposite, with the steep crests in the region where the wind is northward, the eddy momentum flux would have been negative.

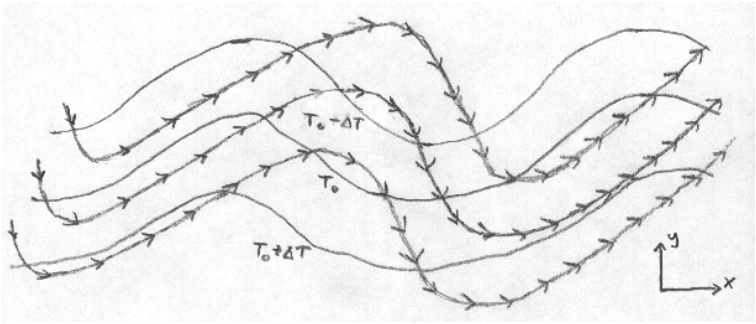

Figure 2.1: *Sketch of a typical planetary wave pattern in the stratosphere. The lines with arrows represent stream lines while and the other lines represent isoterms. The temperature is decreasing towards North.*

Observations of the stratosphere show that mainly planetary waves number 1, 2 and 3 occur in this region. The wave number refers to the number of waves around the Earth along a latitude. As mentioned in section 2.2 changes from the steady state only occur when the forcing terms and circulation terms are out of balance. Thus it is only when the waves are transient that changes in the time-dependent quantities (zonal mean temperature and zonal mean zonal wind) come about. During a development of a wave as the one sketched in figure 2.1 a temperature increase and a negative zonal wind acceleration would be the result. This is the case during the development of sudden stratospheric warmings (Labitzke 1981).

2.4 Gravity waves

Momentum deposition by gravity waves (the X-term in the Eulerian mean equations) has been shown by theory to explain the distribution of temperatures seen in the mesosphere (Andrews et al. 1987). However the basic physics of the momentum deposition is still poorly known (CEDAR 1998) and no general circulation model has of yet obtained reliable results as a very high resolution is needed to model the generation of these waves and as complicated non-linear interactions between the waves themselves and the mean flow occur that is neither well understood (Andrews et al. 1987).

All waves owe their existence to restoring forces. The restoring forces define how the waves behave. In practice gravity waves are normally divided into two groups, buoyancy waves and inertio-gravity waves. Here the first have only the pressure gradient force

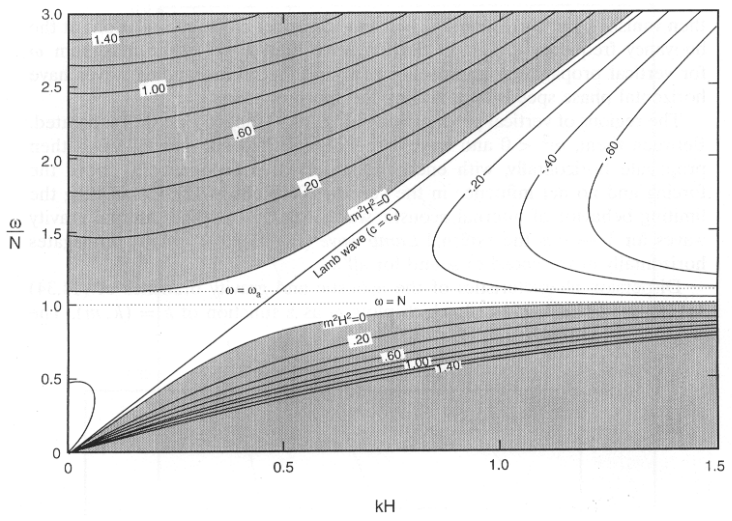

Figure 2.2: *The total solution of the general equations in non-dimensional numbers with respect to gravity waves. If it is assumed that there are no non-linear interactions. The figure is taken from Salby (1996).*

and the gravity force as restoring forces, while the latter also have the Coriolis force as a restoring force. In the upper mesosphere, observations of buoyancy waves have been numerous (Andrews et al. 1987) since the first observation of gravity waves in the ionosphere by Hines (1960).

In the following it will be sought to describe the buoyancy waves, which have frequencies that are much higher than f and thus are not affected by the Coriolis force, with respect to the propagation of these and the theory of Lindzen (1981) on how the gravity waves deposit their momentum in the upper mesosphere.

In figure 2.2 the frequency (ω) and vertical wave number (m) of a gravtity wave are shown as a function of horizontal wave number (k) of the gravity wave. There are three possible solutions for each set of horizontal and vertical wave numbers: The solution in the lower dark area is defined as an internal gravity wave, the solution along the line in the middle is defined as a Lamb wave that propagates with the speed of sound (c_s) and the solution in the upper dark area is defined as an acoustic gravity wave. The figure shows only the the solutions of gravity waves with wavelenghts that are of the order of the atmospheric scale height ($H \approx 10km$). For much shorther wavelengths (these would be to the right on the figure) the acoustic gravity wave would propagate with the speed of sound as a regular sound wave and the internal gravity wave would oscillate with the Brunt-Väisällä frequency. In the following sections internal gravity waves will be considered under the Bossineq approximation, i. e. that the pressure gradient force can be neglected in the horizontal directions. This implies that an air parcel will oscillate with the Brunt-Väisällä frequency and it is thus a good approximation for the

gravity wave with short wavelengths compared to the atmospheric scale height.

2.4.1 Propagation of buoyancy waves

When describing buoyancy waves it is helpful only to have two spatial dimensions to consider. This is achieved by defining the horizontal co-ordinate to always be parallel to the phase velocity of the buoyancy waves. The vertical co-ordinate is the log-pressure co-ordinate (defined in equation (2.1)) as before.

If the governing equations for the perturbation quantities of the buoyancy waves are considered in this co-ordinate system and all perturbations are assumed to have a wave solution of the form $exp(i(kx + mz - \omega t))$, the set of equations can be solved. If the solution is written with the vertical wavenumber (m) isolated, the result is the Taylor-Goldstein equation (Salby 1996)

$$m^2 = \frac{N^2}{(c_x - \overline{u})^2} - k^2 + \frac{\frac{\partial^2 \overline{u}}{\partial z^2}}{c_x - \overline{u}} \tag{2.13}$$

Here k and m are the horizontal and vertical wave numbers respectively, ω is the frequency and c_x is the horizontal phase speed of the wave ($c_x = \omega/k$). Note that the mean horizontal wind ($\overline{u}$) here is not the same as the zonal mean zonal wind defined earlier, due to the definition of the co-ordinate system!

From the Taylor-Goldstein equation information on the vertical propagation of the waves can be deduced. As long as m^2 remains positive the waves can propagate vertically, but if m^2 goes to infinity the vertical wavelength will go to zero and the wave-momentum will be deposited in the mean flow. The height at which this occurs is defined as the critical level. If m^2 goes to zero on the other hand, the vertical wavelength will go to infinity and vertical wavepropagation will cease. The height at which this occurs is defined as the turning level (Salby 1996).

Thus the possibilities at which vertical wave-propagation is impossible are:

1. If N^2 is negative. I. e. the stratification is not stable and no waves occur at all.

2. If a turning level is reached due to either a lowering of the static stability (N^2), a strong negative vertical curvature of the mean horizontal wind ($\frac{\partial^2 \overline{u}}{\partial z^2}$) or a sufficient increase of the horizontal background wind ($\overline{u}$).

3. If a critical level is reached due to the mean wind becoming equal to the wave-phase velocity.

Figure 2.3 shows an example of a turning level due to an increase in the horizontal wind with height. The vertical wavenumber in case 1 goes below zero around 10 km

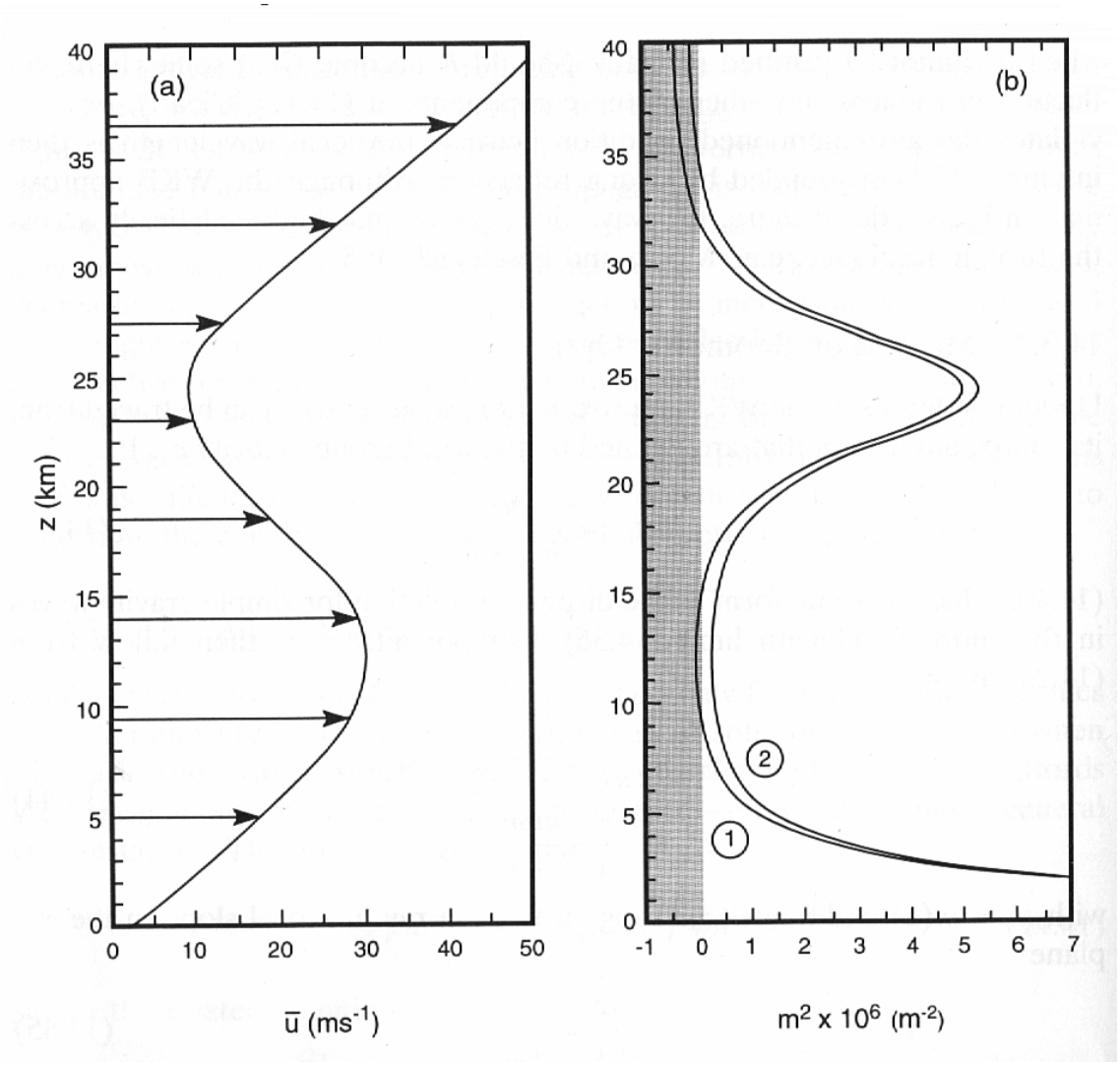

Figure 2.3: *The vertical wave number squared calculated from equation (2.13). Here the horizontal wind is varying with height and the Brunt-Väisällä frequency is constant. Taken from (Salby 1996).*

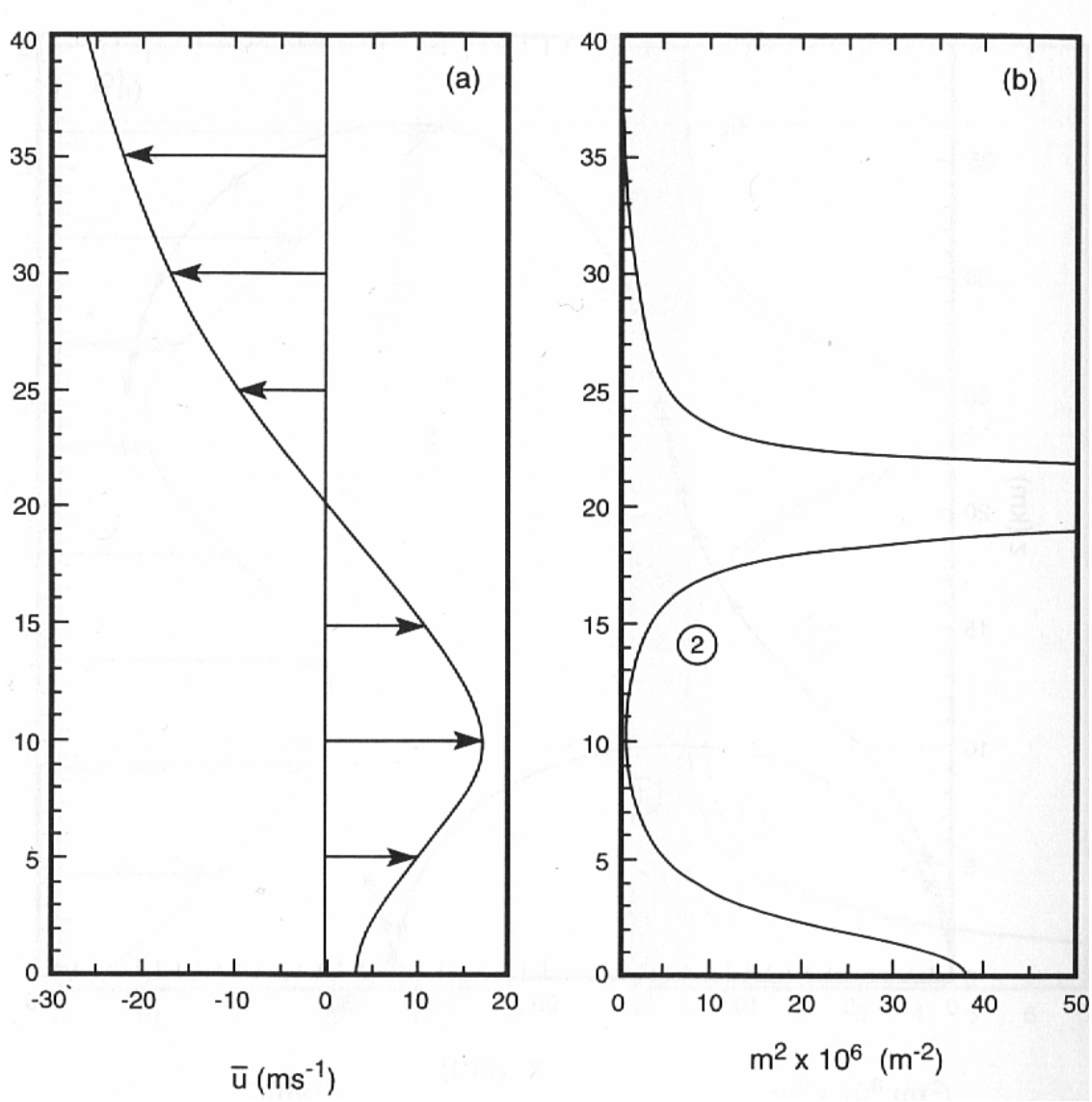

Figure 2.4: *The vertical wave number squared calculated from equation (2.13). As before the Brunt-Väisällä frequency is constant, but the horizontal wind is varying differently. The vertical axis is the height in kilometers as on the previous figure. Taken from (Salby 1996).*

height, while the propagation continues up to 40 km height in case 2. The mathematical claim that the vertical wavelength goes to infinity can be explained physically by considering a wave that is propagating horizontally. Thus the wave at the turning level is reflected downwards.

Figure 2.4 (from Salby (1996)) shows an example of a critical level. The critical level occurs were the mean horizontal velocity goes to zero, as c_x in this case has been chosen to be zero.

2.4.2 Momentum deposition by buoyancy waves in the upper mesosphere

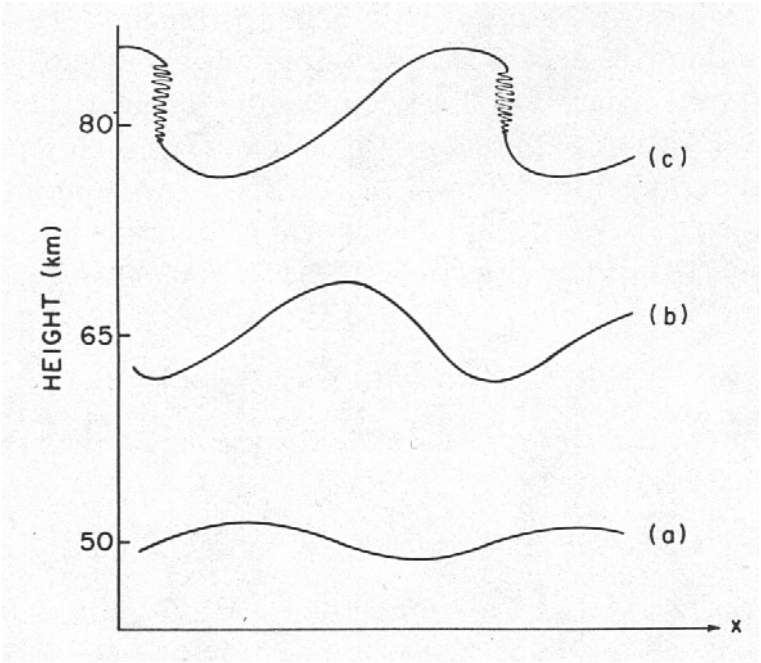

Figure 2.5: *Schematic diagram of vertically propagating internal gravtity waves in the mesosphere. Taken from Salby (1996).*

Lindzen (1981) modeled the buoyancy wave effect on the upper mesospheric flow, as a development from the suggestion of Hines (1965) that breaking buoyancy waves are a heating source in the upper atmosphere. Hines used the fact that the pressure decreases exponentially up through the atmosphere to assume that the perturbation velocities of the waves (the wave amplitudes) are increasing with height, if the kinetic energy of the waves ($\rho u'^2$) is to be constant. Therefore at some height the waves become unstable and break, analogous to ocean waves breaking at the shoreline. Figure 2.5 is a schematic diagram of this. Lindzen showed from a scale analysis that the main effect of the waves on the mean flow is the convergence of vertical momentum flux ($-\rho_0^{-1}\frac{\partial(\rho_0\overline{u'w'})}{\partial z}$) and calculated the expression in equation (2.14) from the assumption

that the turbulent momentum flux is proportional to the wind gradient with the eddy viscosity coefficient (K) as the proportionality factor, i. e.

$$\overline{X}_{uppermesosphere} = -\rho_0^{-1}\frac{\partial(\rho_0\overline{u'w'})}{\partial z} = \frac{N^2K}{c_x - \overline{u}} \tag{2.14}$$

To obtain equation 2.14 Lindzen used the two-dimensional co-ordinate system described in section 2.4.1. Thus there is a vertical wave momentum flux convergence in the direction of the horizontal phase velocity if this is larger than the mean horizontal wind. Now if the horizontal phase velocity is westward it would mean a vertical wave momentum flux divergence in equation (2.8) due to the different definitions of co-ordinate systems.

Lindzen's theoretical consideration on the gravity wave effects in the upper mesosphere implies a large zonal forcing of the zonal mean circulation, which can explain the departure of the upper mesospheric temperatures from radiative equilibrium temperatures (Andrews et al. 1987).

From the observational fact that non-radiative heating is seen at a large height interval in the mesosphere, i. e. it does not seem to be only at a specific height, but rather above a specific height. Lindzen made the hypothesis that the waves do not break completely but rather break continuously at the fringes when they propagate above this specific height.

Briefly described the gravity wave induced heating of the winter-pole mesosphere occurs as follows:

- Gravity waves propagate from the troposphere as the wind in winter is eastward in both the troposphere and the stratosphere and waves that propagate toward the west do not reach critical levels (section (2.4.1)).
- The waves that reach the upper mesosphere are then mainly westward propagating and deposit zonal momentum in the negative direction (section (2.4.2)).
- The decrease in momentum in the zonal direction will cause an increase in the meridional velocity (equation (2.8)).
- If it is assumed that no gravity waves are created over the North Pole, there will be a negative meridional gradient of the meridional wind velocity that must be balanced by a positive gradient in the vertical wind velocity (equation (2.7)), which again means increasing adiabatic heating with height (equation (2.10)).

3 The OH rotational spectrum

Excited OH-molecules in the upper mesosphere are created from the reactions:

$$O_3 + H \longrightarrow OH^*(v' \leq 9) + O_2 + 3.3eV \tag{3.1}$$

$$HO_2 + O \longrightarrow OH^*(v \leq 6) + O_2 + 2.3eV \tag{3.2}$$

where the two reactions are equally important in the polar night over Svalbard according to Sivjee and Hamwey (1987) . Their model calculations on the OH^* chemistry positions the OH^*-layer around 85 km height, which is in good agreement with OH^* in-situ measurements made with rockets that in average have found the height of the layer to be 87 km and the thickness to be 8 km (Baker & Stair, Jr. 1988).

The ozone in the first reaction is created from a three-body reaction with O and O_2. Thus advection of O and H is needed in order to keep the concentration of OH^* constant. Myrabø and Deehr (1984) found that a meridional wind of 20 m/s is necessary.

Airglow spectra are created when molecules excited into higher vibrational and rotational states go to lower molecular states. The spectra consist of vibrational bands, which again are made up of rotational lines.

In order to derive the rotational temperatures, the goal of measuring the spectra, it is necessary to produce synthetic spectra. For this purpose knowledge about line strength and line wavelength is needed. While the wavelength is only dependent on the energy of a state-to-state transition, the line intensity is somewhat more complicated to infer. As this is dependent on both the transition probability and the number of molecules in the initial state.

The energy loss of a transition between an upper and a lower molecular state determine the emission wavelength of a diatomic molecule. The upper and lower states can differ in vibrational, rotational and translational states. OH^* in the upper mesosphere is in its translational ground state $X_2\Pi$ making the wavelength of an emission (Herzberg 1950)

$$\lambda = hc/(E_{v'} - E_{v''} + E_{J'} - E_{J''}) = (G(v') - G(v'') + F(J', v') - F(J'', v''))^{-1} \tag{3.3}$$

where $G(v)$ is defined as the vibrational term in vibrational state v, $F(J, v)$ is the rotational term in rotational state J and vibrational state v, h is Planck's constant, c is the speed of light in vacuum and E is the energy of the states. $'$ and $''$ mark the upper and lower quantum state respectively.

The vibrational term for OH(6-2) is, with vibrational constants taken from Krassovsky (1962):

$$G(v) = \omega_e(v+1/2) - \omega_e x_e(v+1/2)^2 + \omega_e y_e(v+1/2)^3 \ldots \tag{3.4}$$

$$\omega_e = 3739.90cm^{-1},\ \omega_e x_e = 84.965cm^{-1},\ \omega_e y_e = 0.598cm^{-1}$$

From the difference between G(6) and G(2) the main wavelength of the band can be found to be 829.46 nm.

The rotational terms are

$$F_1(J,v) = B_v(J+1/2)^2 - \Lambda^2 + 1/2\sqrt{4(J+1/2)^2 + Y_v(Y_v-4)\Lambda^2} - D_v J^4 \tag{3.5}$$

$$F_2(J,v) = B_v(J+1/2)^2 - \Lambda^2 - 1/2\sqrt{4(J+1/2)^2 + Y_v(Y_v-4)\Lambda^2} - D_v(J+1)^4 \tag{3.6}$$

$$B_v = 18.867cm^{-1} - 0.708cm^{-1}(v+1/2) + 0.00207cm^{-1}(v+1/2)^2 \ldots$$

$$D_v = 0.00018cm^{-1},\ Y_v = -7.553 - 0.3039v - 0.01158v^2 \ldots$$

As it may be noticed, there are two rotational terms. This is due to the fact that the electron spin can be either up or down. Also, another splitting of these lines occur due to the so-called λ-type doubling. This is an effect of the rotation of the nuclei. But this doubling is of no importance at the resolution used in these measurements.

Not all rotational transitions are possible. From the selection rule it is known that they only occur when ΔJ is -1, 0 or 1 giving rise to the P-, Q- and R-branch of the vibrational band (Herzberg 1950).

The intensity of a line in photons$\cdot s^{-1}$ is a product of the number of molecules in the upper state and the transition probability to end up in the lower state

$$I_{v',J' \to v'',J''} = N_{v',J'} A_{v',J' \to v'',J''} \tag{3.7}$$

Here the prime ($'$) and the double prime ($''$) are again symbols for the upper and lower state respectively.

The transition probabilities are also called Einstein coefficients. The distribution of rotational levels in a certain vibrational state is defined by the Boltzmann distribution, if the molecules are in thermodynamical equilibrium. Thus making the number of molecules in the upper state

$$N_{v',J'} = \frac{N_{v'} 2(2J'+1)\exp(-F(J')hc/kT_{rot})}{Q_R}, \tag{3.8}$$

$$Q_R = 1 + 3\exp(\frac{-2B_v hc}{kT_{rot}}) + 5\exp(\frac{-6B_v hc}{kT_{rot}}) + \cdots \approx \frac{kT_{rot}}{hcB_v} \tag{3.9}$$

T_{rot} is the rotational temperature, Q_R is the partition function and k is Boltzmanns constant. If the assumption of thermodynamical equilibrium is fulfilled T_{rot} must be equal to the temperature of the surroundings.

Pendelton et al. (1989) questioned whether OH^* is in thermal equilibrium. They made spectral measurements of the OH(7-4)-band and came to the conclusion that for rotational levels above $J' = 5$ this is not the case. In general whether OH^* is in thermal equilibrium or not is a question of vibrational level, as the lifetime of the excited molecule decreases when the vibrational level increases. The collision frequency in this altitude of the atmosphere is of the order 10^{-2} s^{-1}, while the average lifetime of OH^* in vibrational state 6 is of the order 10^{-4}-10^{-3} s (Turnbull & Lowe 1989).

Thus it would seem that there are other bands with lower upper vibrational states that are better for deriving the temperature. This does however not seem to be the case. Other factors have to be taken into consideration. The band should be in a wavelength region where clouds do not stop it and contamination from auroral bands should be avoided as far as possible. It is also an advantage to use a band that is situated at a high wavelength, as the Rayleigh scattering is decreasing with increasing wavelength. Therefore OH(6-2) is an optimal band for deriving the temperature.

The only problem that remains is that there are two unknowns ($N_{v'}$ and T_{rot}) in the equations. Therefore it is only possible to calculate the relative strengths of the lines. In practice these unknowns are derived by the aid of synthetic spectra. These are fitted by the least squares fit-method to the measured spectra. The basis for calculating these is the term values of Krassovsky (1962) and the Einstein coefficients of Turnbull and Lowe (1989), which are used as input values in the Delphi program SyntheticOH that is described in section 5.

4 Experimental

The Ebert-Fastie spectrometer is set up at the auroral station in Adventdalen, Svalbard (78°N, 15°E). The spectrometer was used to measure the OH(6-2) vibrational band. From such measurements the temperatures of the neutral atmosphere surrounding the layer of excited OH can be found, as described in section 3. The spectrometer is shown in figure 4.1.

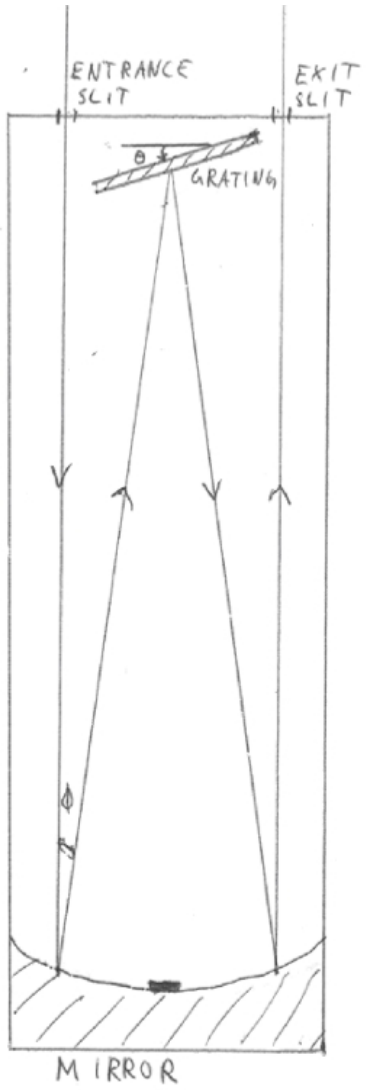

Figure 4.1: *A sketch of the Ebert-Fastie spectrometer with the light path added*

An Ebert-Fastie spectrometer is a monochromator. A monochromator measures the intensity of radiation at specific wavelengths. It consists of a spherically concave mirror, a plane reflective grating, and a pair of curved slits. The setup is shown in Figure 2.1. Ebert invented it in 1889 and it was later adjusted by Fastie (1952a & b),

who added the curvature to the slits in order to adapt these to the spherical aberration of the mirror. The mirror is used to make the incoming rays parallel before they hit the grating and to focus the outgoing rays onto the exit slit. The central region of the mirror has been painted black to obstruct light from going directly from the entrance slit to the exit slit. The grating is used to disperse the light so that only one narrow wavelength region will reach the exit slit. The slits are made as narrow as possible in order to get high spectral resolution. In other words, throughput and resolution are dependent on each other.

Which wavelength line that goes through the spectrometer is dependant on the grating equation

$$n \cdot \lambda = a(\sin\alpha + \sin\beta), \quad n = 1, 2, 3, \ldots \tag{4.1}$$

Here n is the order, λ is the wavelength, a is the spacing between the grating grooves, α and β are the angles of incidence and reflection respectively. The angles are measured from the grating normal. The grating is blazed to maximize the amount of light that reaches the exit slit. A blazed grating is a grating on which the grooves are manufactured in a way that the direction of maximum interference between waves at a specific wavelength is the same as the direction of a specific order of defraction for the specific wavelength. On the spectrometer used in this case, the grating is blazed to the first order of defraction.

In order to make this equation useful for an Ebert-Fastie spectrometer the equation must be rewritten using θ and ϕ as defined in figure 4.1 and figure 4.2. As it can be seen ϕ is a constant that is dependent on the slit to slit distance and the distance along the optical axis from the mirror to the center of the grating. Substituting these two angles into the grating equation gives

$$n \cdot \lambda = 2a \sin\theta \cos\phi \tag{4.2}$$

Thus making the wavelength dependent on the grating angle (θ), the instrument constant (ϕ), the grating groove spacing a and the spectral order (n).

The specifications of the instrument used are:

Parameter	Value
Focal length (f)	1 m
Instrument constant (ϕ)	3.6°
Grating groove spacing (a)	833 nm

On the Ebert-Fastie spectrometers the grating angle of the instrument is variable.

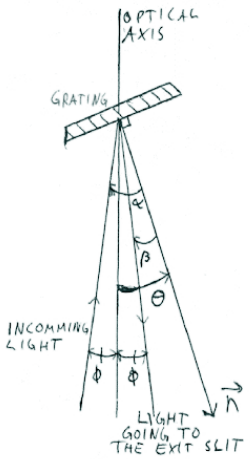

Figure 4.2: *Sketch of the light path at the grating, with the angle definitions included. The vector n is the normal to the grating plane.*

This opens up the possibility of scanning through several wavelengths. In practice, connecting the grating mount to a rotating cam with a mechanical arm, does this. The cam is a sinus drive. It is shaped to make sure that the scan is linearly in wavelength.

Replacing the cam (shown in figure 4.3) opens the opportunity to change the total spectral range span.

Differentiating the grating equation with respect to the wavelength, and dividing by the focal length, gives an expression for the band pass. The band pass (BP) is defined as the full width at half maximum of a spectral line at the exit slit. This equals the product of the entrance slit width (w) and the linear dispersion ($d\lambda/dx$)

$$BP \equiv \frac{d\lambda}{dx}w = \frac{a\cos\beta}{n \cdot f}w = \frac{a\cos(\theta - \phi)}{n \cdot f}w \tag{4.3}$$

The band pass should be as high as the minimum resolution required for the specific task. Thus the slits are as wide as possible and the instrument gathers the optimal light amount. To separate the lines in the OH(6- 2) band a band pass of 0.5nm is needed. The setup of the instrument after being optimized for OH(6-2) is

Parameter	Value
Slit width (w)	0.6mm
Band pass(BP)	0.48nm
Grating angle(θ)	31,5° – 33,0°
Scan rate	25s
Field of view	5.0°
Spectral range	831.2nm – 874.5nm

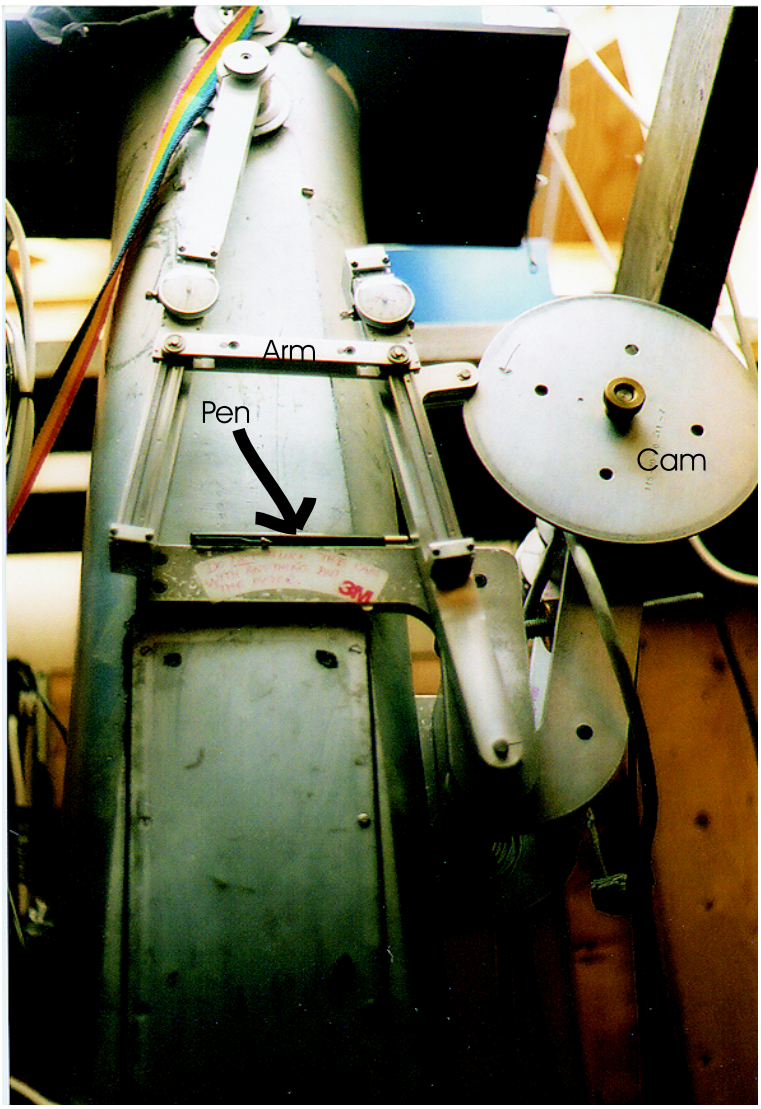

Figure 4.3: *The cam on the Silver Bullet spectrometer and the arm that is connected to the grating in the top of the spectrometer. A pen is placed on the spectrometer to give an indication of the size.*

As mentioned earlier the wavelength going through the spectrometer is dependent on the order. In this case the first order is used. This does not mean that all other orders are avoided though. From equation (4.2) it can be seen that incoming light with first order wavelengths at 1/2, 1/3, 1/4 ... of the spectral range will overlap the first order light. Therefore it is necessary to put a high frequency (low wavelength) cut off filter in front of the entrance slit.

A sharp cut red filter is used, cutting off all light with wavelengths below 620 nm. In the Near infrared region the filter absorbs 12% of the incoming light.

In order to measure the intensity of the light at the exit slit, a photomultiplier tube (PMT) is used. In this case the Hamamatsu R943-02. This uses the photoelectric effect (Einstein 1921) to generate a current from light. The PMT consists of a photocathode and an anode coupled by a set of small plates multiplying the original photoelectrons from the photocathode to obtain a stronger current.

The current from the PMT is directed through a pulse amplifier and discriminator (PAD), which converts the pulses of electrons into clean, five-volt pulses of equal length (Hamamatsu 1993). These then go to a PC that counts the number of pulses during a specified integration period and stores the results.

A high voltage difference between the cathode and anode is needed in order to get the photomultiplying effect to work. This has a side effect. Currents will be running in the system even though no light reaches the photocathode! These will cause so-called dark counts that will be seen as a certain level of random noise below the signal, noise that makes the measurements inaccurate. The number of dark counts depends on the temperature. I.e. the higher temperature the more dark counts. Therefore the PMT is cooled to a temperature of -20°C. Even though, dark counts are not avoided and these have to be considered. As the dark counts are random, summing several spectra reduces the noise effect of these.

The number of pulses from the PMT is not the same as the amount of photons reaching the detector at the specific wavelength. Light is lost in the instrument due to optical aberrations and due to the efficiencies of the grating, mirror, filter and the detector. In practice these efficiencies are difficult to estimate. Therefore a so-called absolute calibration is carried out. The calibration factors for the wavelengths are found by measuring the spectrum of a lamp with known intensity. However the relative sensitivity over the OH(6-2) wavelength region is constant, so an absolute calibration is not necessary in this case (Viereck 1989).

5 Spectral analysis

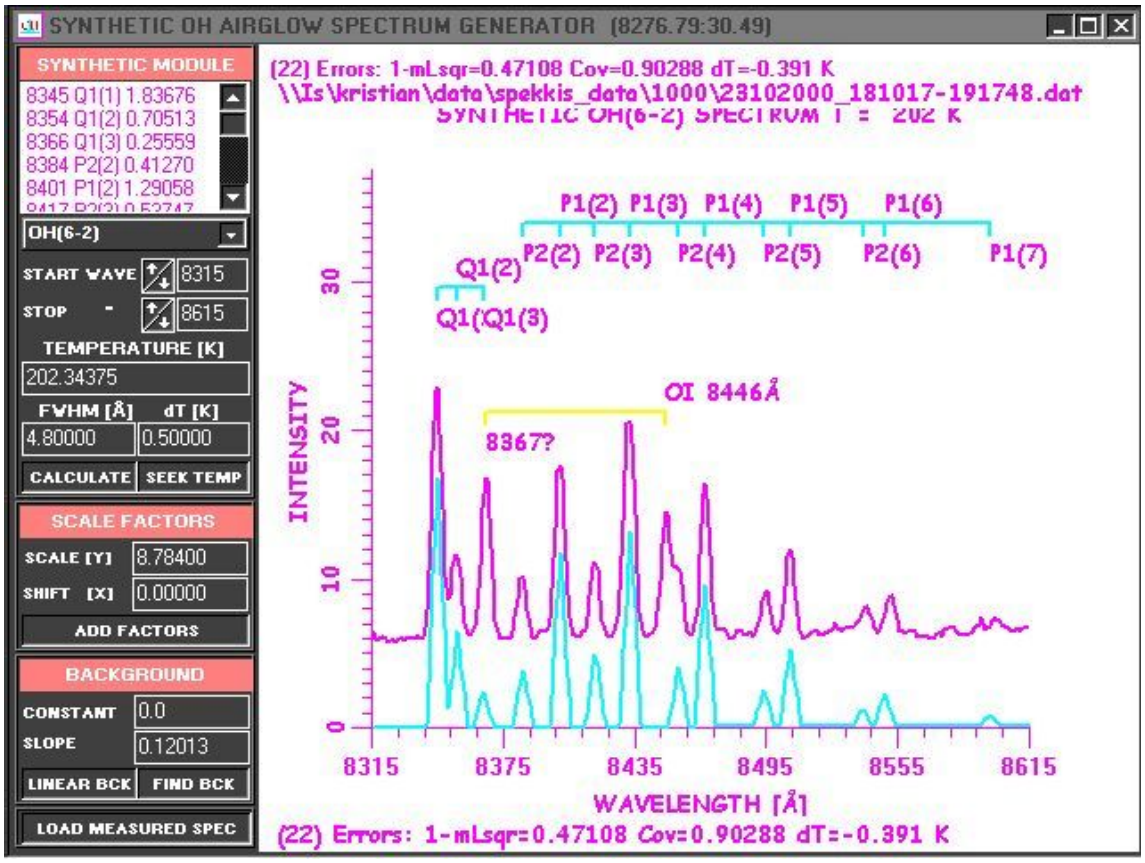

Figure 5.1: *The SyntheticOH-interface.*

The spectral analysis was done in three steps:

1. The poorest spectra were sorted away.
2. 1 hour averaged spectra were calculated.
3. The rotational temperatures were calculated.

The sorting was performed by the aid of the IDL program spekkis.pro (copyright Sigernes 1993). Using "spekkis" the emission intensities could be plotted as a function of wavelength and time, making it easy to see when the data were good and when they were not. By the term "good" is meant whether the following analysis of the rotational temperatures gave satisfactory results, which according to Viereck (1989) is a FIT-function higher than 0.8. He defined the FIT-function as

$$FIT = \frac{100 - l}{100} \tag{5.1}$$

Here l is the least square-error between the measured and the synthetic spectrum. Viereck found that a FIT-function of 0.8 corresponded to a standard deviation of $\pm$ 2 K.

After the first temperature analyses it was clear that no useful temperature estimations could be obtained during strong magnetic substorms or storms, as the auroral contamination from NO molecules in the thermosphere increases in strength and variability over the entire spectral region. The NO emissions are the main contributors to the OH(6-2) background when the sky is clear. In comparison the level of the dark counts is around 1, if the arbitrary intensity scale on figure 5.1 is used. As a rule of thumb it was found that if the background rises to more than three times of strength to the strongest of the hydroxyl lines no reliable temperatures could be obtained. The same rule applied to cloud-scattered light from the moon or from Longyearbyen. "Good" measurements were obtained even at time where the sky was overcast, a fact that is explained in the discussion. Another feature making the data "bad" were strong electric pulses coming through the electric system at the auroral station, giving false signals to the counting card in the computer.

After sorting the data the "good" spectra were averaged over one hour, in order to get the noise from the NO background and the noise originating from the aberrations of the spectrometer as low as possible. At times with optimal conditions even better time resolution could be obtained with low error. However as this limits the number of days with good measurements, it was chosen to use the one-hour averages.

The calculation of the temperatures themselves was done with the Delphi program SyntheticOH.exe (Sigernes & Nielsen 2000). As mentioned in section 3 the rotational lines originating from states higher than J'=5 are not in thermal equilibrium for the (7-4) vibrational band (Pendelton et al. 1989). Therefore the lines above this rotational state were not used for the calculation of the temperatures. All of these lines are in thermal equilibrium in the OH(6-2) vibrational band, as the OH (7-4) excited molecule has a shorter lifetime than the OH (6-2) excited molecule due to the higher upper vibrational state. So the upper rotational states that are in thermal equilibrium for the OH (7-4) excited molecule are also for the OH (6-2) excited molecule. Therefore only the first eight lines of the P-branch were considered in the analysis even though measurements of four more lines were done. By running the SyntheticOH program it could be seen that lines from other atoms/molecules contaminated parts of the spectra. Theses lines were the atomic oxygen line at 844.6 nm and a line at 836.7 nm that is the vibrational band (4-3) of ionized Nitrogen molecules.

All the lines in the vibrationally excited OH-spectrum has been written into the file TOTAL_QUANT.INC that is used by SyntheticOH.exe together with their respective upper and lower rotational state numbers and Einstein coefficients.

The SyntheticOH-program is described in the help file of the program. Briefly what was done when the synthetic spectra are fitted to the measure spectra was:

1. The spectrum was calibrated (normally not necessary, as the spectrometer already is wavelength calibrated.)

2. The background data points were read and from these a linear background was calculated.

3. The synthetic spectrum was iterated to fit the measured spectrum.

The linear background was estimated as follows:

1. The data file was loaded.

2. The synthetic spectrum was splined to the new data set. Splined means that the discrete wavelengths in the synthetic spectrum were set to equal those in the data file.

3. For all wavelengths in the spectrum, it was checked whether they were one of the wavelengths in TOTAL_QUANT.INC. If they were, a temporary intensity value was assigned to them.

4. For all wavelengths, a convolution value was assigned if they were within 1 band-pass of a line. The convolution is necessary due to the width of the exit slit of the spectrometer.

5. For all wavelengths that were not yet assigned with a value the background values were set equal to the measured values at the respective points in the spectrum.

6. From the background values that then were defined a linear regression was made.

7. The intercept- and slope-values from this regression were then used to estimate the background values at the spectral lines.

After defining the background values in the synthetic spectrum the synthetic spectrum could be fitted to the measured spectrum by an iteration that ran as follows:

1. The initial temperature was set to 150 K, the initial temperature step was set to 50K and the minimal temperature step was set to the desired value.

2. Again the wavelengths from TOTAL_QUANT.INC and the convolution of these were defined.

3. The number of molecules in the upper state was set to an initial value calculated from the formula:

$$N_{v'} = \frac{I_{j=j(Imax)} - Background_{j=j(Imax)}}{A_{v'J' \to v''J''} 2(J'+1) \exp\left(\frac{-F(J'v')hc}{kT}\right) Q_R^{-1}} \tag{5.2}$$

The values in the formula all being as defined in section 3 except the I term and the background term that are the maximum intensity of the OH(6-2) band in the synthetic spectrum as it was defined during the last run of the program and the background value at the same wavelength respectively. The synthetic spectrum was always stored to give initial values for the next run of the program. The rotational term was calculated in the module EnergyTerms.inc, by equation 3.5 or 3.6, using the output values J and v as read from TOTAL_QUANT.INC as input values.

4. The intensities of the OH(6-2) lines were calculated from equations 3.7 and 3.
5. The intensities of the synthetic spectrum were calculated by adding the background values.
6. The mean least square error was calculated between the measured and the synthetic spectrum and was then assigned to the variable Q0.
7. The temperature was then assigned to the variable T0 and a new temperature was obtained by adding the temperature step value.
8. Steps 2 to 5 were repeated and a new mean least square error was assigned to the variable Q1.
9. If now Q1 was less than Q0, i. e. the new fit was better, the temperature step was set equal to -(T-T0)/2. If not, i. e. the new fit was worse, the temperature step was not changed.
10. The steps 6 to 9 were repeated until either QO was larger than 0.99, the temperature step was less than the earlier defined minimum temperature step or the loop had run 200 times.

In the following figures (5.2–5.4), the graphical output of SyntheticOH is shown for the various phases of the iteration process. The first figure shows an example of an initial synthetic spectrum calculated from a temperature of 125 K. The second figure shows the synthetic spectrum after the background has been fitted. The third figure shows the final fit, in this case corresponding to a temperature of 202 K. When figure 5.2 is observed with the knowledge that the rotational temperature in the measured spectrum is 202 K, the modulation of the OH(6-2) spectrum with respect to temperature variations can be evaluated. As it can be seen the relative difference in intensity

between the synthetic and the measured spectrum is increasing for the last six lines of the p-branch showing that fewer molecules are found in the higher rotational states at lower temperatures. It can also be seen that the ratio between the emission strength from the molecules with a spin-up electron and the molecules with a spin-down electron is larger for the synthetic spectrum with the relatively low temperature (hint: the lines are alternating between "spin up lines" and "spin down lines").

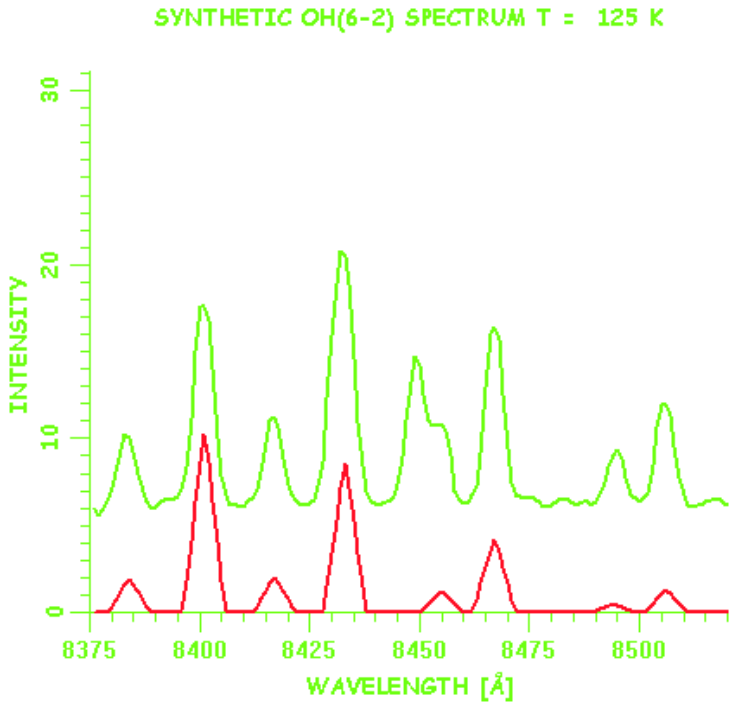

Figure 5.2: *An example of a measured spectrum (the green curve) and the synthetic spectrum for $T = 125$ K (the red curve). The intensity units are arbitrary.*

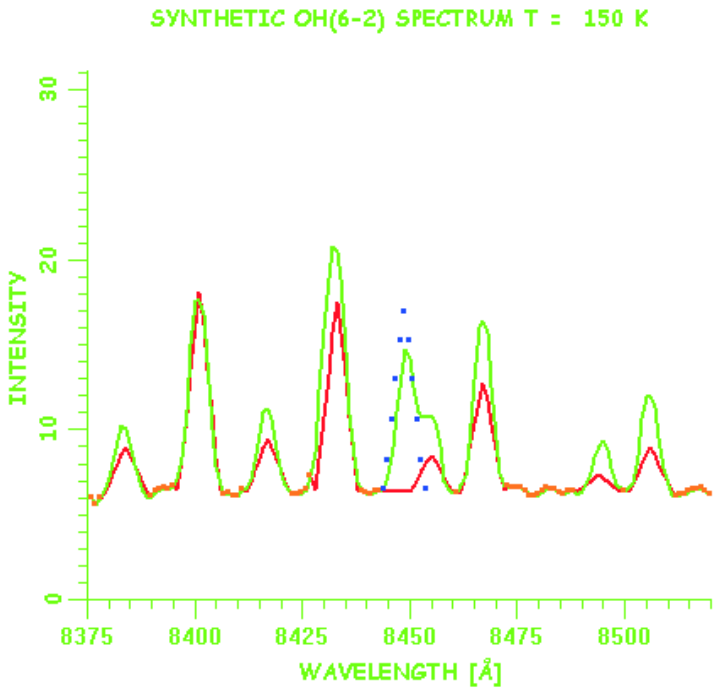

Figure 5.3: *The same measured spectrum as in the previous figure. Now with a synthetic spectrum for $T = 150$ K, and a fitted background.*

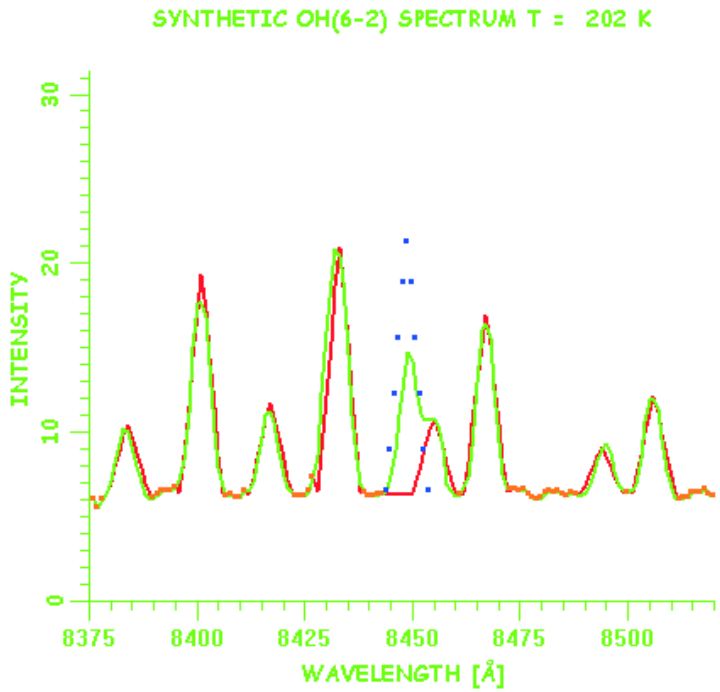

Figure 5.4: *The same measured spectrum as in the previous figures. Now the iteration is finished and the rotational temperature has been found to be 202 K.*

6 Results

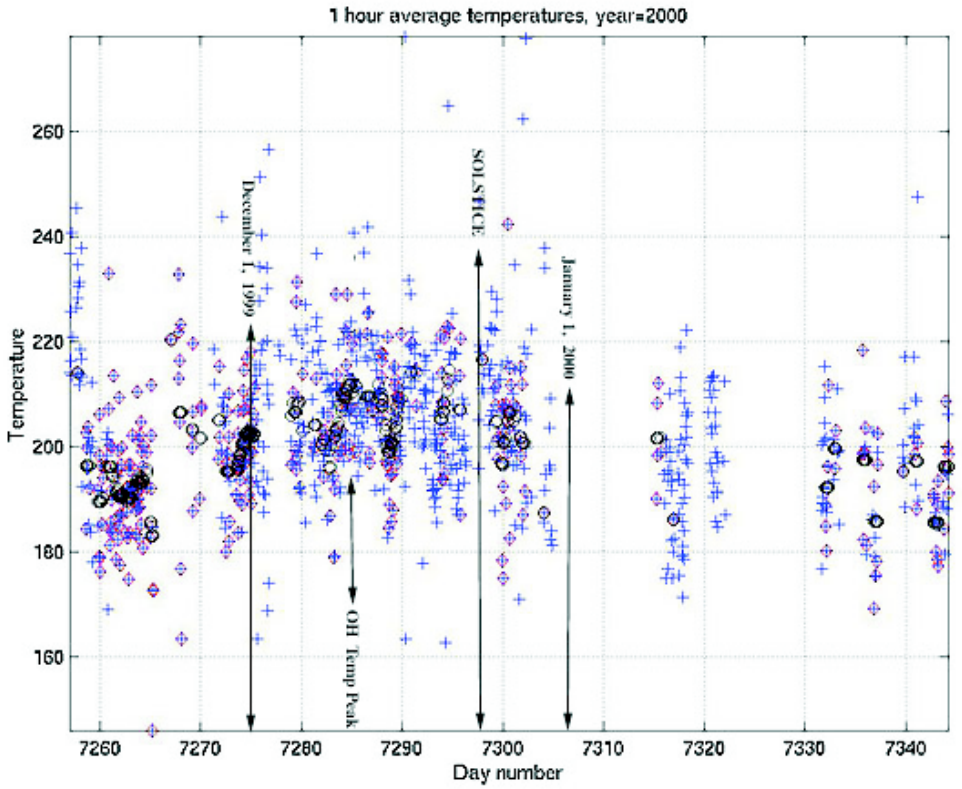

Figure 6.1: *The OH-rotational temperatures in the 2000 winter. The x-axis is in day number from day 1, the 1st of January 1980. The temperatures are marked with blue crosses. The temperatures with mean least square-errors better than 0.8 are also marked with red diamonds. The black circles represent a 24-hour running mean of the temperatures.*

6.1 The OH-rotational temperatures through the 1999-2000 winter

The measurements were started on Svalbard on the 13th of November and lasted until the 6th of February 2000. In figure 6.1 the temperatures calculated for the winter 1999 are shown. The 24-hour running mean of the temperatures on the figure were calculated with the computer program Allread.m that was programmed in Matlab 5. The 24-running mean was calculated as the average of all temperatures within $\pm$ 12 hours. The code of the program can be found in appendix B. As explained in section 3 the OH-airglow temperatures are the same as the average of neutral air temperatures in a layer of 8 km halfwidth at approximately 87 km height.

In some periods there are only a few temperatures and in some there are no temperatures. In these periods either cloud-scattered moonlight or problems with electrical noise have made the measurements impossible or bad. The moon was above the horizon in the periods from the 19^{th} of November to the 3^{rd} of December, from the 16^{th} of December to the 30^{th} of December and from the 12^{th} of January to the 27^{th} of January. That the moon is above the horizon is not a direct problem for measuring the OH(6-2) emissions, as these are measured in the zenith and the moon never rises very far above the horizon at Svalbard. However when the sky is cloudy the moonlight is scattered into the spectrometer making the background intensity rise in both strength and variability, which makes the fit of the synthetic spectrum poor. The electrical noise-problem was present throughout January, where almost no good measurements could be made. At some times the electrical noise was constant and at other times in the form of strong pulses.

The average temperature in the middle of November was around 190 K, then it rose to 210 K and stayed around this temperature between the 5^{th} and the 20^{th} of December. In the end of January and in the beginning of February it again dropped to around 195 K. By observing the running mean temperature, there are some indications of variations with periods of around five days. None of these are however statistically significant.

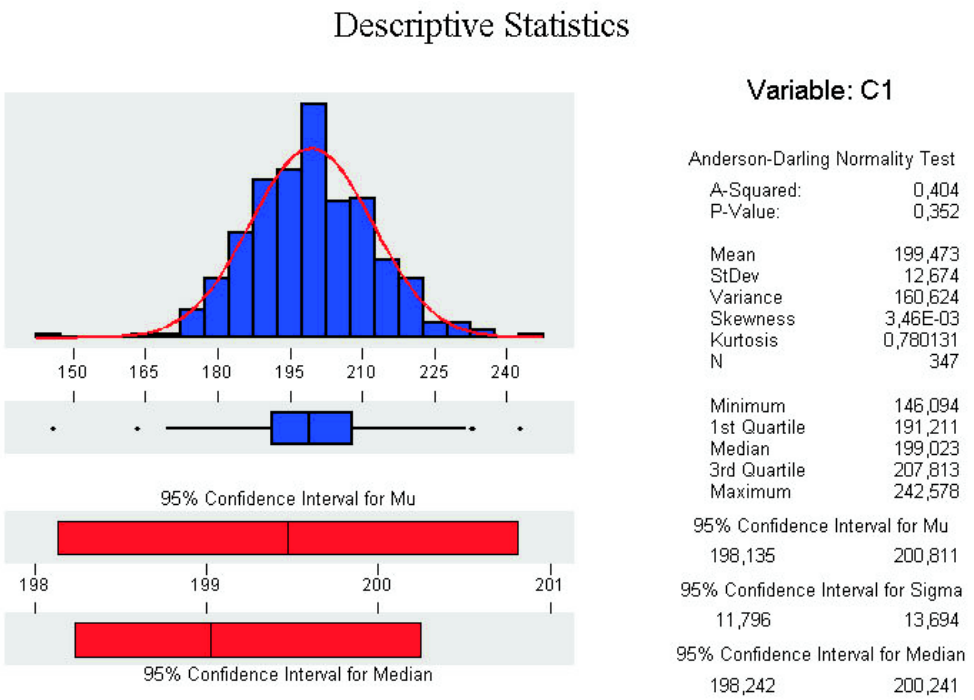

Figure 6.2: *The statistics of the hourly OH-rotational temperatures*

The distribution of the hourly temperatures is shown in figure 6.2. These are

normally distributed with a standard deviation of 13 K. The extreme values of the distribution are 146 K in the low end and 243 K in the high end.

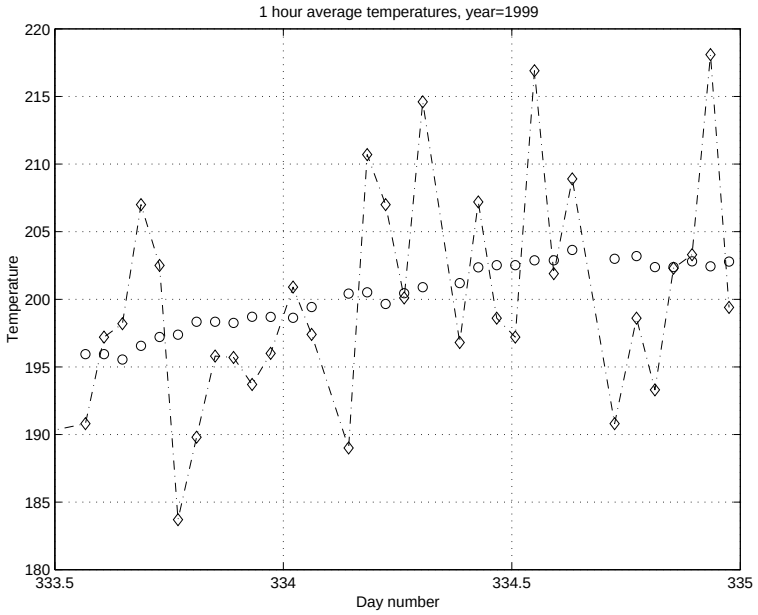

Figure 6.3: *The hourly averaged OH-airglow temperatures on the 30^{th} of November (day number 334) 1999. Again the diamonds represent hourly averaged temperatures with a mean least square-error better than 0.8 and the circles represent a 24-hour running mean.*

An example of the temperature variations within a day is shown in figure 6.3. As it can be seen the variations are not resolved, i. e. the main frequency of the variations are higher or around 1 hour. It can also be seen that the average temperature can change by more than 20 K within 1 hour.

6.2 The stratospheric variations in the 1999-2000 winter

In general the winter 1999-2000 was characterized by a stable polar vortex in the lower and middle stratosphere with much lower temperatures averaged over December and January, than in any previously observed Arctic winter (Manney & Sabutis 2000). In the middle stratosphere the vortex intensified throughout November and reached a maximum in the middle of December, with the geopotential height difference at 30 hPa inside and outside the vortex increasing from $1.2 \cdot 10^3 m$ on the 15^{th} of November to $1.7 \cdot 10^3 m$ on the 15^{th} of December. The vortex remained at this maximum strength fairly constant until the beginning of January, whereafter it again weakened.

Daily means of the temperatures and geopotential heights in the stratosphere from the last 35 years until December 1999 were kindly supplied by the stratospheric research group in Berlin. From these data the horizontal winds in the stratosphere can be

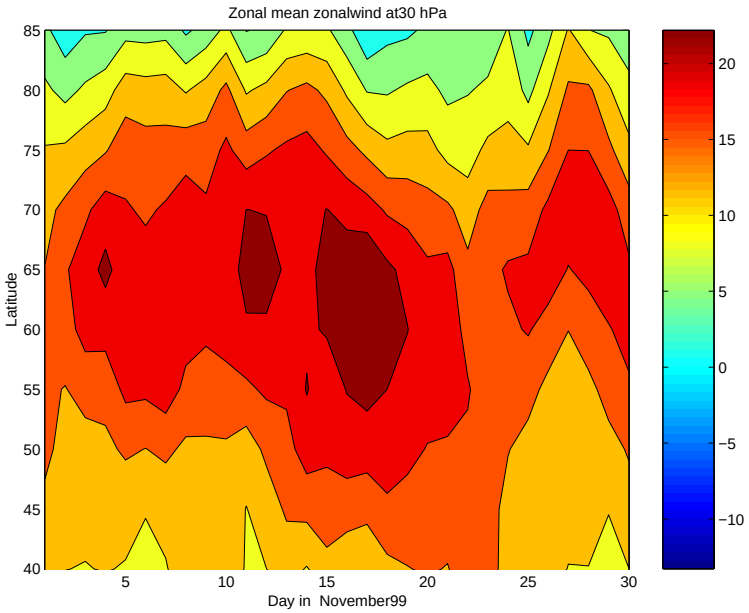

Figure 6.4: *The zonal mean zonal wind in m/s during November 1999 from 40° N to the North Pole.*

calculated by the assumption of geostrophy (Equations (6.1) and (6.2)), which is a good assumption in the stratosphere.

$$u_g(\lambda,\phi,p) = -\frac{1}{a\ g_0 f}\frac{\partial Z(\lambda,\phi,p)}{\partial \phi} \approx -\frac{(Z(\lambda,\phi+5^\circ,p) - Z(\lambda,\phi-5^\circ,p))}{a\ g_0 f\ 10^\circ} \tag{6.1}$$

$$v_g(\lambda,\phi,p) = \frac{1}{a\ cos(\phi) g_0 f}\frac{\partial Z(\lambda,\phi,p)}{\partial \lambda} \approx \frac{(Z(\lambda+5^\circ,\phi,p) - Z(\lambda-5^\circ,\phi,p))}{a\ cos(\phi) g_0 f\ 10^\circ} \tag{6.2}$$

The Berlin data were in the co-ordinates longitude (λ), latitude (ϕ) and pressure level (p), which are used in the equations above. The other variables are: Z the geopotential height, f the planetary vorticity, g_0 the global average of gravity at mean sea level and a the radius of the Earth. The horizontal resolution of the data was 5° x 5°.

The data from the stratospheric research group of Berlin was evaluated using various home made Matlab 5-programs. These can be seen in the appendices C, D, E, F, G and H.

On the 23^{rd} of November a small stratospheric warming occurred. In figure 6.5 the geopotential height distribution over the northern hemisphere is shown on this day. As it can be seen an asymmetric wave number 1 is developing. In figure 6.4 and figure 6.6 it can be seen that the perturbation actually has the effect described in section 2, as the zonal mean temperature is increasing and the zonal mean zonal wind is decreasing during the development of the asymmetric wave.

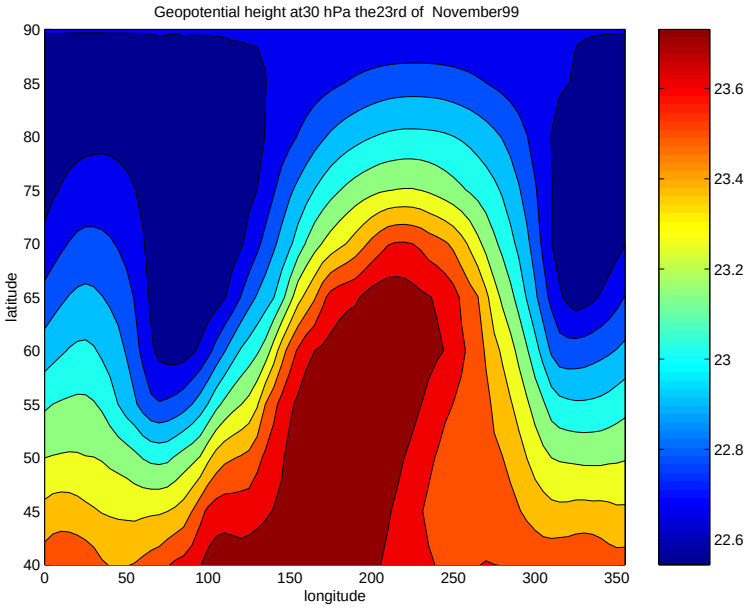

Figure 6.5: *The Geopotential height in kilometers at a height of 30 hPa for the entire northern hemisphere from 40° N to the North Pole on the 23rd of November 1999.*

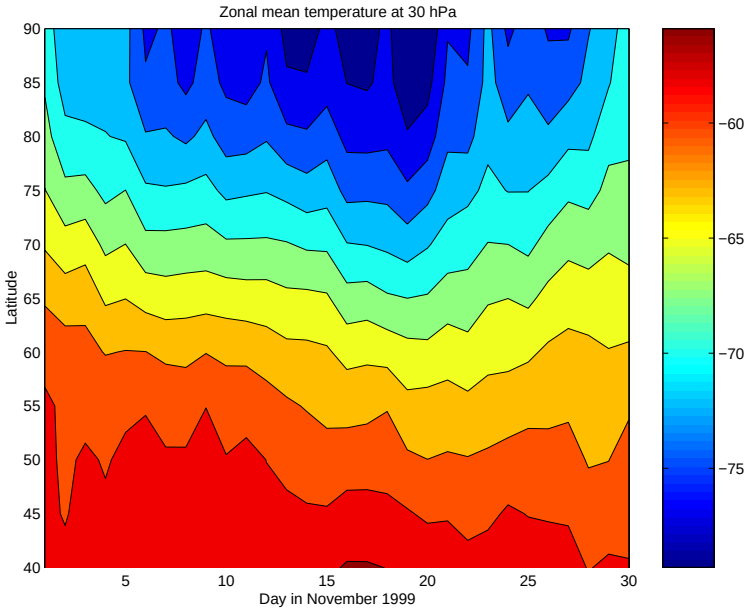

Figure 6.6: *The zonal mean temperature in November 1999 from 40° N to the North Pole.*

6.3 Variations in the outgoing longwave radiation

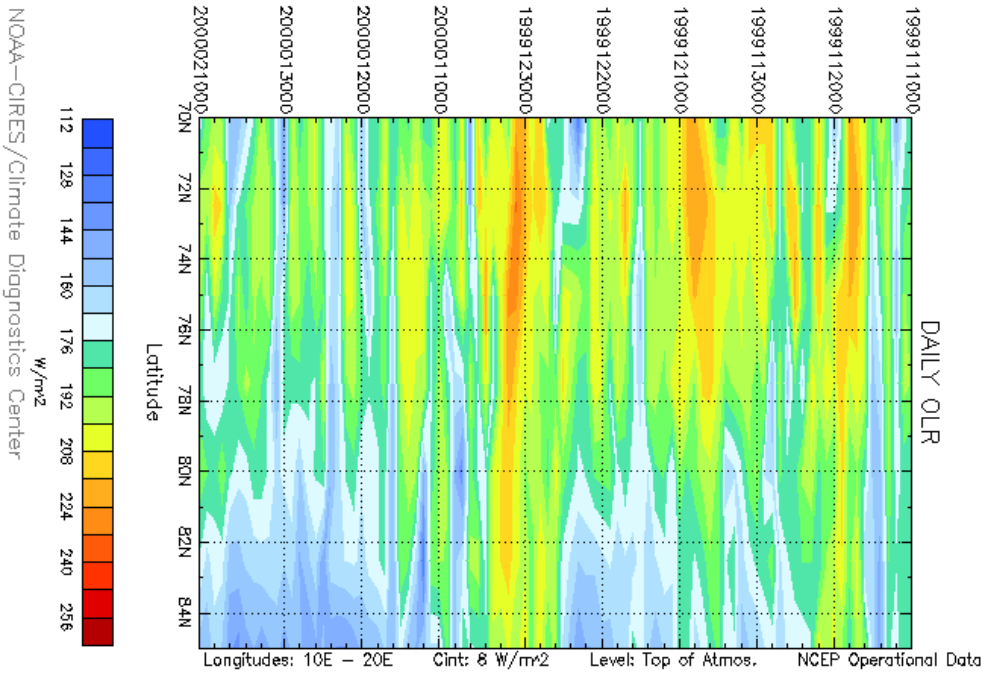

Figure 6.7: *Interpolated outgoing longwave radiation at the top of the atmosphere over Svalbard, calculated from archive-data of the National Center of Atmospheric Research (NCAR). The data are from the winter 1999/2000. The time tick marks on top of the figure are in the format: year month day hour.*

During the wintertime strong variations in the longwave radiation coming from the ground exist. These are mainly due to changes in the tropospheric cloud distribution and also occur due to the changes in the ground temperature. The outgoing longwave radiation over Svalbard is shown in figure 6.7. The data in the figure is provided by the NOAA-CIRES Climate Diagnostics Center, Boulder, Colorado, from their Web site at http://www.cdc.noaa.gov/. It has been averaged over the longitudinal band between 10°E and 20°E and is thus a good representative for the outgoing longwave radiation reaching the OH-airglow layer over Svalbard. As it can be seen the outgoing longwave radiation varied from $150 W/m^2$ to almost $220 W/m^2$. The minimum values are of course due to thick cloud cover and the maximum values occur when there are no clouds.

7 Discussion

7.1 Uncertainties in the measurements and analysis

The sky over Svalbard is often cloudy and so it was also in the winter of 1999/2000. This raises the question whether reliable OH-airglow temperatures can be measured when the sky is cloudy. Especially since many temperatures were found that had an acceptable fit even when the sky was completely overcast. Thus the OH-airglow emissions in the near infrared can penetrate the clouds. However it could be expected that the extinction of radiation over the OH(6-2) wavelength region evaluated (837.5 nm – 856.0 nm) is uneven, which would cause either a relative increase or decrease in extinction with respect to wavelength and thereby a false temperature estimation.

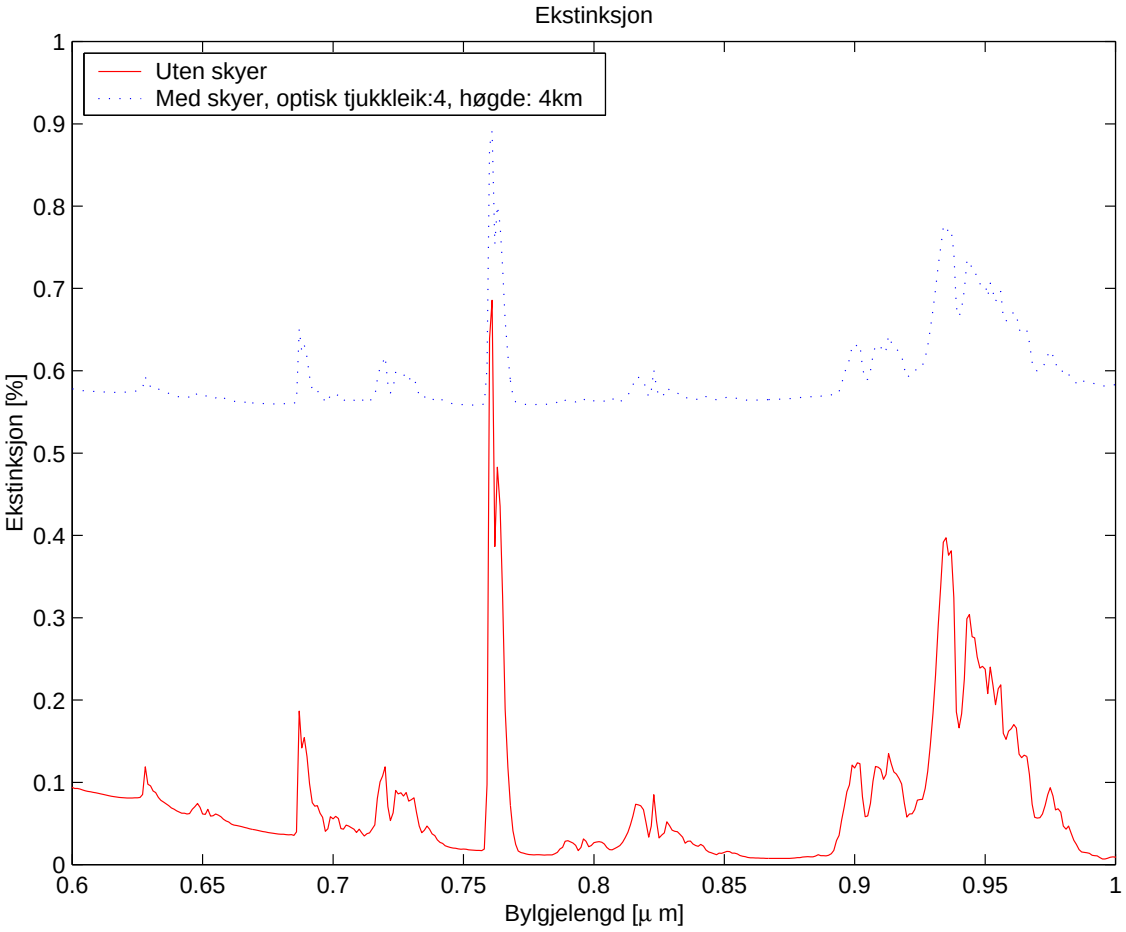

Figure 7.1: *The atmospheric extinction of radiation from the zenith for an arctic atmosphere with clouds (the blue curve), and without clouds (the red curve) as a function of wavelength in micrometers. The figure is taken from (Dagestad 2001).*

In figure 7.1 results from an atmospheric radiation model are shown that have been

made by the radiation group at the Geophysical Institute in Bergen (Dagestad 2001). As it can be seen there are large relative variations in the extinction in the model even with a clear sky. This is mainly due to the absorption of atmospheric water vapor in the troposphere. There is in fact a small variation in the extinction of the OH(6-2) emissions, when the sky is clear: At 830 nm the extinction is around 5 % while it drops to around 1 % at 860 nm.

To test how big an error this atmospheric modulation causes, the extinction factors have been used to reconstruct the original OH(6-2) spectrum (equation (7.1)).

$$I_{original}(\lambda) = \frac{I_{measured}(\lambda)}{1 - extinction(\lambda)} \tag{7.1}$$

The test was performed on the same spectrum as was used for the analysis demonstration in section 5. The temperature of the corrected spectrum was calculated to be 201 K or 1 K colder than the temperature calculated for the uncorrected spectrum. The lowest standard deviation that has been observed in the temperatures this far was 4 K on a day in October 2000 with almost no gravity wave activity. Therefore it does not seem necessary to use the extinction factors in the OH-airglow analysis. For the model atmosphere with a thick cloud cover it can be seen on figure 7.1 that the relative variation in extinction in fact is less over the OH(6-2) vibrational spectrum when the sky is overcast! Of course only half the photons (if the scattered ones are not accounted for) reach the spectrometer, so the measurements are of worse quality, but there is no reason to disregard the measurements made when the sky was overcast.

Another but smaller error seen in the measurements is that the convolution of the lines in the synthetic spectrum does not completely resemble the shape of the measured lines. These seem to be slightly broader at the base (e. g. figure 5.4), which has the effect that the fringes of the lines are assigned to be background values. As the fringes of the lines have consistently higher intensity values than the background the estimation of the background is slightly wrong, something that should be accounted for in future versions of SyntheticOH.

7.2 Discussion of the hourly temperature variations

Temporal variations due to the buoyancy waves would be an explanation for the large variability of the temperatures at frequencies that seem to be around one hour. But is it possible that gravity waves can cause changes of more than 20 K within an hour? How large vertical perturbations are actually needed to cause such large temperature variations?

This question can be addressed when it is considered that the air parcel motions caused by gravity waves must be nearly adiabatic. For adiabatic motion it is known that $\frac{T}{p^{(\gamma-1)/\gamma}}$ is constant. Where γ is the ratio between the specific heat capacities at

constant pressure and volume that for the atmosphere is approximately 1.4. Now the pressure change needed to induce a rise in temperature of 25 K can be calculated

$$\frac{p_2}{p_1} = \left(\frac{T_2}{T_1}\right)^{\gamma/(\gamma-1)} = \left(\frac{225}{200}\right)^{3.5} = 1.51 \tag{7.2}$$

Thus the height perturbation needed to cause the observed variations in temperature is somewhere between 2 and 3 kilometers, which does not seem unlikely.

7.3 Discussion of the general (seasonal) temperature variation

Several factors can be expected to affect the temperatures of the OH-airglow layer on a longer time scale. Sources of energy come from absorption of infrared (longwave) radiation by carbon dioxide, adiabatic heating due to forced downward motion and heating due to absorption of incoming ultraviolet radiation by molecular oxygen. During the polar night of course only the two first contributions need to be considered. The main energy sink is outgoing longwave radiation from carbon dioxide molecules. Here it must be kept in mind that the heating effect of carbon dioxide is small in comparison to the cooling effect (Brasseur & Solomon 1986). Thus the average temperature is a balance between the radiative cooling and heating and any temperature change forced by vertical motion, for instance the vertical motion that would be expected due to westward gravity wave drag at mid-latitudes (see section 2.4.2 and figure 1.6).

In section 2.4.1 it was shown that the background wind in the atmosphere has a large effect on the gravity wave propagation. The waves with phase velocities equal to the mean wind will meet critical levels. This is believed to be the reason why the gravity wave drag in the mesosphere is mainly westward or opposite to the wind direction in the stratospheric jet (Holton 1982).

When it is also taken into consideration that the gravity waves mainly occur in fairly broad spectra (i. e. they are rarely monochromatic), it seems logical to assume that changes in the strength of the stratospheric jet are responsible for changes in the strength of the mesospheric mid-latitude gravity wave drag. Changes in the strength of the mid- latitude gravity wave drag again causes changes in the vertical wind according to the equations (2.8) and (2.7), which from equation (2.10) causes changes in the temperature.

In equation (2.9) the mean zonal wind is only dependant on the meridional gradient of the geopotential height. As the geopotential height in November and December 1999 at 50 hPa and 30hPa height in the re-analysis data varied much more at the North Pole than at lower latitudes, it is a good assumption to make that the mean zonal wind in the jet at these heights is proportional to the geopotential height at the North Pole. On this background the hypothesis that the long period temperature variations in

the OH- airglow temperature were dependent on the stratospheric polar geopotential heights was tested. In figure 7.2 and figure 7.3 the resulting regressions are shown. The regression was made of daily temperature averages from days with six or more temperatures with error-functions better than 0.8.

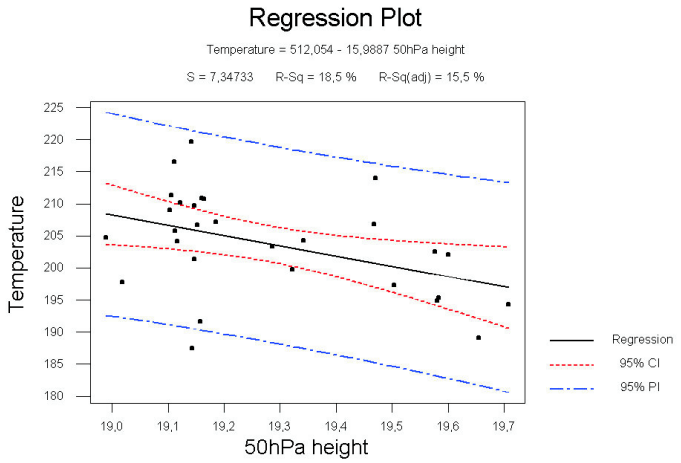

Figure 7.2: *Regression of the daily averaged OH-airglow temperatures from November and December 1999 against the polar geopotential height in km at the 50 hPa pressure level.*

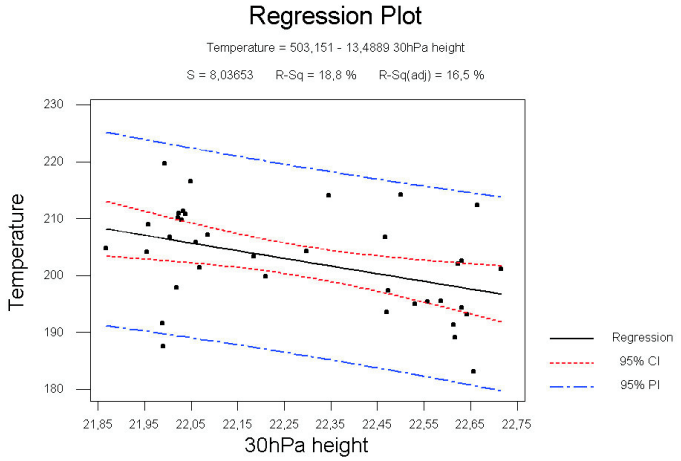

Figure 7.3: *Regression of the daily averaged OH-airglow temperatures from November and December 1999 against the polar geopotential height in km at the 30 hPa pressure level.*

The stippled red lines on the figures show the 95 % confidence interval of the regression line and the blue lines show the 95 % prediction interval. As it can be seen the regression gave the expected result and the hypotheses were both approved with test probabilities of 2.0% and 0.7% respectively.

The implication of these regressions is that mid-latitude zonal mean zonal wind in the stratosphere is statistically connected to the polar OH-airglow temperatures. When the zonal mean zonal wind at 50 hPa and 30 hPa increase so do the temperatures in the OH-airglow over Svalbard. Presumably due to the critical level filtering of parts of the gravity wave spectrum as suggested by Lindzen (1981) and Holton (1982) & (1983).

7.4 Sources of gravity waves

In October 2000 measurements were done with the SOUSY-Svalbard RADAR of the Max-Planck Institute of Aeoronomy. From these RADAR measurements the vertical winds in the troposphere and lower stratosphere could be estimated with high accuracy and resolution in time. The RADAR measurements contained many good examples of tropospheric internal gravity wave generation. During a few of the days strong vertical motions of more than 1 m/s were seen that persisted for several hours in the air column over the RADAR (Pers. comm. Röttger 2000). Such vertical wind speeds are typical for standing mountain lee waves. The wind on these days was weak from either North or East. Thus very stable air from the ice-covered sea North and East of Svalbard was advected over the steep mountains of Svalbard. This should be excellent conditions for generation of mountain lee waves (see figure 1.4) (Wurtele, Sharman & Datta 1996). On the days without mountain lee wave activity smaller oscillations were observed with periods around 15 minutes, i. e. the Brunt-Vaisällä period. These seemed to be generated at a height of a few kilometers, and could thus be the results of shear instability in the flow (Pers. comm. Röttger 2000).

It is unknown which of these types of internal gravity waves that are of the greatest importance for the gravity wave drag in the mesosphere. From equation (2.13) it can however be speculated that waves with higher horizontal wavenumbers meet turning levels at higher wind speeds. Thereby such waves can propagate to higher altitudes than waves with lower horizontal wavenumbers. Small scale waves generated by shear instability in the flow of the troposphere, would have a large impact on the mesospheric flow if they would maintain their kinetic energy, due to the large decrease in atmospheric density.

Gravity waves can also be generated by strong convection. In the summer of 1999 a group of researchers from the University of Alaska, Fairbanks were looking for signs of electrical discharges over thunderclouds with a high speed camera. The camera was equipped with a CCD-detector that was sensitive in the visible and near infrared spectral regions. Thus the camera could see not only the electric discharges over the thundercloud (sprites), but also variations in the OH-airglow layer. A pattern of concentric rings traveling away from the center of convection with high velocity was clearly seen (Pers. comm. Heavner 2000). The phase speed of these waves indicated

that these were clearly acoustic gravity waves (see section 2.4 for the definition of acoustic gravity waves).

7.5 Is there any effect of the daily variations in outgoing longwave radiation?

In section 6.3 it was shown that there were variations of up to 20 % from the mean in the outgoing longwave radiation at the top of the atmosphere over Svalbard during the winter 1999/2000. These large variations affect the heating in the atmosphere around the OH-airglow layer due to absorption of carbon-dioxide molecules of longwave radiation.

Therefore the hypothesis that the outgoing longwave radiation affects variation in the OH- airglow temperature was tested. As in the previous test daily averages were used. The regression is shown in figure 7.4

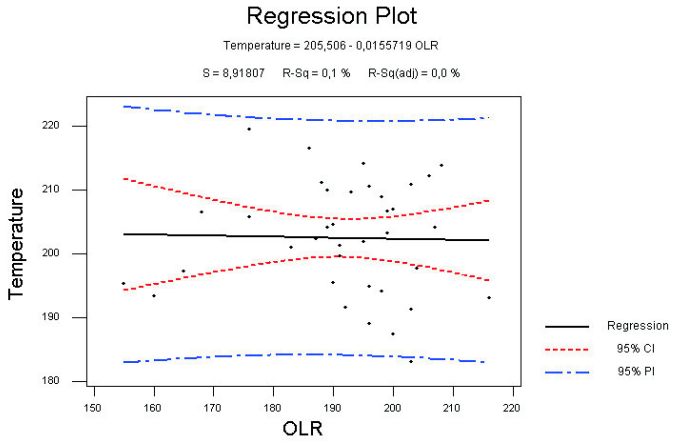

Figure 7.4: *Regression of the daily averaged OH-airglow temperatures from November and December 1999 against the outgoing longwave radiation in W/m^2 at (78° N, 15° E).*

The hypothesis was rejected with a test probability of 88.9 %.

7.6 Comparison with the results published earlier

In general the OH-airglow temperatures measured in the winter 1999/2000 have the same morphology as the earlier measurements described in the introduction: The hourly variations shown in figure 6.3 have amplitudes of ± 20 K, similar to those described by (Myrabø 1984), and the seasonal variation is also in good agreement with the seasonal variations described by (Myrabø 1986). Neither any obvious indications of a connection with the geomagnetic activity were noticed during the winter, allthough no detailed study of this was made.

However the temperature is lower in the winter 1999/2000 (by approximately 10 K) compared to the winters in the early eighties described by Myrabø (1986). This could be an indication of the cooling in the upper mesosphere observed by Golitsyn et al. (1996), Ulich & Turunen (1997) and Bremer (1997) and modeled by e. g. Berger and Dameris (1993) and Akmaev and Fomichev (1998), but further investigation of the dependence of the OH-rotational temperatures to the variations in the winds in the lower atmosphere is needed to certify this, as the temperature difference also could be a result of a weaker stratospheric jet.

References

Akmaev, R. A. & Fomichev, V. I. (1998), 'Cooling of the mesosphere and lower thermosphere due to doubling of CO_2', *Ann. Geophys.* **16**, 1501–1512.

Andrews, D. G., Holton, J. R. & Leovy, C. B. (1987), *Middle Atmosphere Dynamics*, Academic Press, Orlando, Florida.

Baker, D. J. & Stair, Jr., A. T. (1988), 'Rocket measurements of the altitude distributions of the hydroxyl airglow', *Physica Scripta* **37**, 611–622.

Berger, U. & Dameris, M. (1993), 'Cooling of the upper atmosphere due to CO_2 increases: a model study', *Ann. Geophys.* **11**, 809–819.

Blackmon, M. L., Geisler, J. E. & Pitcher, E. J. (1983), 'A general ciculation model study of january climate anomaly patterns associated with interannual variation of equatorial pacific sea surface temperatures', *J. Atmos. Sci.* **40**, 1410–1425.

Brasseur, G. & Solomon, S. (1986), *Aeronomy of the middle atmosphere*, D. Reidel Publishing Company, Dordrecht, Holland.

Bremer, J. (1997), 'Long-term trends in the meso- and thermosphere', *Adv. Space Res.* **20**(11), 2075–2083.

Brewer, A. W. (1949), 'Evidence for a world circulation provided by the measurements of helium and water vapour distributions in the stratosphere', *Quart. J. Roy. Met. Soc.* **75**, 351.

CEDAR (1998), 'CEDAR phase III-report: cedarweb.hao.ucar.edu/docs/cedar.pdf'.

Chapman, S. (1930), 'On ozone and atomic oxygen in the upper atmosphere', *Phil. Mag.* **10**, 369.

Dagestad, K. F. (2001), Sammenhengen mellom reflektert TOA radians og globalstråling ved bakken, Master's thesis, The Geophysical Institute, the University of Bergen, Norway.

Deehr, C. S., Sivjee, G. G., Egeland, A., Henriksen, K., Sandholt, P. E., Smith, R., Sweeney, P., Duncan, C. & Gilmer, F. (1980), 'Ground-based observations of F-region associated with the magnetospheric cusp', *J. Geophys. Res.* **85**, 2185.

Dobson, G. M. B. (1930), 'Observations of the amount of ozone in the Earth's atmosphere and its relation to other geophysical conditions', *Proc. Roy. Soc. London* **129**(Sec. A), 411.

Duck, T. J. (2000), *CEDAR Workshop on Polar Mesospheric Dynamics*, http://www.haystack.mit.edu/ tomduck/cedar_ws/.

Duck, T. J., Whiteway, J. A. & Carswell, A. I. (1998), 'LIDAR observations of gravity wave activity and arctic stratospheric vortex core warming', *Geophys. Res. Lett.* **25**(15), 2813.

Dunkerton, T. J. & Baldwin, M. P. (1992), 'Modes of interannual variability in the stratosphere', *Geophys. Res. Lett.* **19**(1), 49–52.

Dunkerton, T. J., Delisi, D. P. & Baldwin, M. P. (1988), 'Distribution of major stratospheric warmings in relation to the quasi-biennual oscillation', *Geophys. Res. Lett.* **15**(2), 136–139.

Einstein, A. (1921), The photoelectric effect, *in* 'Nobel Laureates', The Royal Swedish Academy of Sciences, Stockholm.

Fastie, W. G. (1952*a*), 'Image forming properties of the Ebert monochromator', *J. Opt. Soc. Am.* **42**, 647.

Fastie, W. G. (1952*b*), 'A small plane grating monochromator', *J. Opt. Soc. Am.* **42**, 641.

Fels, S. (1985), 'Radiative-dynamical interactions in the middle atmosphere', *Adv. Geophys.* **28A**, 277–300.

Gadsden, M. (1998), 'The North-West Europe data on noctilucent clouds: a survey', *J. of Atmos. and Solar-Terr. Phys.* **60**, 1163–1174.

Gage, K. S. (1979), 'Evidence for a $k^{-5/3}$ law internal range in mesoscale turbulence', *J. Atmos. Sci.* **36**, 3850.

Golitsyn, G. S., Semenov, A. I., Shefov, N. N., Fishkova, L. M., Lysenko, E. V. & Perov, S. P. (1996), 'Long-term temperature trends in the middle and upper atmosphere', *Geophys. Res. Lett.* **23**, 1741–1744.

Hamamatsu (1993), *How To Use Photon Counting Unit C3866, Operation Manual*, Hamamatsu Photonics K. K., Japan.

Herzberg, G. (1950), *Spectra of Diatomic Molecules*, D. Van Nostrad co., inc. New Y.

Hines, C. O. (1960), 'Internal atmospheric gravity waves at ionospheric heights', *Can. Jour. Phys* **38**, 1441.

Hines, C. O. (1965), 'Dynamical heating of the upper atmosphere', *J. Geophys. Res.* **70**, 177.

Holton, J. R. (1982), 'The role of gravity wave induced drag and diffusion in the momentum budget of the mesosphere', *J. Atmos. Sci.* **39**, 791.

Holton, J. R. (1983), 'The influence of gravity wave breaking on the general circulation of the middle atmosphere', *J. Atmos. Sci.* **40**, 2497.

Holton, J. R. (1992), *An Introduction to Dynamic Meteorology, Third Edition*, Academic Press, Orlando, Florida.

Kodera, K. & Yamazaki, K. (1990), 'Long-term variation of upper stratospheric circulation in the northern hemisphere in december', *J. Metor. Soc. Japan* **68**, 101–105.

Krassovsky, V. I., Shefov, N. N. & Yarin, V. I. (1962), 'Atlas of the airglow spectrum 3000–12,400 Å,', *Planet. Space Sci.* .

Kvifte, G. I. (1959), 'Night glow observations at Ås during the I. G. Y.', *Geophys. Norvegica* **20**, 1.

Labitzke, K. (1981), 'Stratospheric-mesospheric midwinter disturbances: A summary of observed characteristics', *J. Geophys. Res.* **86**(C10), 9665–9678.

Labitzke, K. & van Loon, H. (1997), 'The signal of the 11-year sunspot cycle in the upper troposphere-lower stratosphere', *Space Sci. Rev.* **80**, 393–410.

Labitzke, K. & van Loon, H. (1999), 'The global range of the stratospheric decadal wave. Part II: The QBO effect on the global stratosphere in the northern winter', *Tellus* **submitted**.

Lastovicka, J. (1989), 'Early major stratospheric warming and the ionosphere over central europe in december 1987', *International Journal of Geomagnetism and Aeronomy* **29**(4), 545.

Lindzen, R. S. (1981), 'Turbulence and stress owing to gravity wave and tidal breakdown', *J. Geophys. Res.* **86**, 9707–9714.

London, J. (1980), Radiative energy sources and sinks in the stratosphere and mesosphere, *in* A. Eiken, ed., 'Proceedings of the NATO Advanced Study Institute on Atmospheric Ozone: Its Variation and Human Influences', Vol. Report FAA-EE-80-20, pp. 703–721.

Lübken, F.-J. (2000), 'Nearly zero temperature trend in the polar summer mesosphere', *Geophys. Res. Lett.* **27**(21), 3603–3606.

Manney, G. L. & Sabutis, J. L. (2000), 'Development of the polar vortex in the 1999-2000 arctic winter', *Geophys. Res. Lett.* **27**(17), 2589–2592.

Matsuno, T. (1971), 'A dynamical model of the stratospheric sudden warming', *Jour. Atmos. Sci.* **28**(13), 1479.

McLandress, C. & McFarlane, N. A. (1993), 'Interaction between orographic gravity wave drag and forced stationary planetary waves in the winter northern hemisphere middle atmosphere', *J. of the Atmos. Sci.* **50**(7), 1966–1990.

Meinel, A. B. (1950), 'OH emission bands in the spectrum of the night sky', *Ap. J.* **111**, 555.

Mirtov, B. A. (1961), *Gaseous Composition of the Atmosphere and Its Analysis*, Izdatel'stvo Akademii Nauk SSSR, Moskva.

Myrabø, H. K. (1984), 'Temperature variation at mesopause levels during witner solstice at 78°N', *Planet. Spa. Sci.* **32**(3), 249–262.

Myrabø, H. K. (1986), 'Winter-season mesopause and lower thermosphere temperatures in the northern polar region', *Planet. Spa. Sci.* **34**(11), 1023–1029.

Myrabø, H. K. & Deehr, C. S. (1984), 'Mid-winter hydroxyl night airglow emission intensities in the northern polar region', *Planet Space Sci.* **32**(3), 263–271.

Myrabø, H. K., Deehr, C. S. & Lybekk, B. (1984), 'Polar cap OH airglow rotational temperatures at the mesopause during a stratospheric warming event', *Planet Space Sci.* **32**(7), 853–856.

Myrabø, H. K., Deehr, C. S. & Sivjee, G. G. (1983), 'Large-amplitude nightglow OH(8-3) band intensity and rotational temperature variations during a 24-hour period at 78°N', *J. Geophys. Res.* **88**(A11), 9255.

Myrabø, H. K., Deehr, C. S. & Viereck, R. (1987), 'Polar mesopause gravity wave activity in the sodium and hydroxyl airglow', *J. Geophys. Res.* **92**(A3), 2527.

Nielsen, K. P., Deehr, C. S., Raustein, E., Gjessing, Y. & Sigernes, F. (2001), 'Polar OH-airglow temperature variations in the 87/88 winter', *Physics and Chemistry of the Earth* **26**.

Nielsen, K. P., Röttger, J. & Sigernes, F. (2001), 'Simultaneous measurements of temperatures in the upper mesosphere with an Ebert-Fastie spectrometer and a VHF meteor RADAR on Svalbard (78°N, 16°E)', *Geophys. Res. Lett.* **28**.

Pancheva, D., Lastovicka, J. & de la Morena, B. A. (1991), 'Quasi-periodic fluctuations in ionospheric absorption in relation to planetary activity in the stratosphere', *Jour. At. Terr. Phys.* **53**(11/12), 1151–1155.

Pendelton, W., Espy, P., Baker, D., Steed, A., Fetrow, M. & Henriksen, K. (1989), 'Observation of OH meinel (7,4) P(N" = 13) transitions in the night airglow', *Jour. of Geophys. Res.* **94**(A1), 505–510.

Salby, M. L. (1996), *Fundamentals of Amospheric Physics*, Academic Press, San Diego, California.

Scherlag, R. (1952), 'Die explosionsartigen stratosphärenwärmungen des spätwinters, 1951-1952', *Ber. Deut. Wetferdienst* **38**, 51.

Sigernes, F. & Nielsen, K. P. (2000), *Computer Program: A synthetic hydroxyl spectrum generator for Windows*, Arctic Research Consultants Ltd.

Sivjee, G. G. & Hamwey, R. M. (1987), 'Temperature and chemistry of the polar mesopause OH', *Jour. of Geophys. Res.* **92**(A5), 4663–4672.

Stephenson, J. A. E. & Scourfield, M. W. J. (1992), 'Ozone depletion over the polar caps caused by solar protons', *Geophys. Res. Lett.* **12**(24), 2425–2428.

Turnbull, D. N. & Lowe, R. P. (1989), 'New hydroxyl transition probabilities and their importance in airglow studies', *Planet. Spa. Sci.* **37**(6), 723–738.

Ulich, T. & Turunen, E. (1997), 'Evidence for long-term cooling of the upper atmosphere in ionosonde data', *Geophys. Res. Lett.* **24**(9), 1103–1106.

van Loon, H. & Labitzke, K. (1999), 'The signal of the 11-year solar cyle in the global stratosphere', *J. of Atmos. and Solar Terr. Phys.* **61**, 53–61.

van Loon, H. & Shea, D. J. (2000), 'The global 11-year solar signal in July-August', *Geophys. Res. Lett.* **27**(18), 2965–2968.

Viereck, R. A. (1989), Effects of gravity waves on the polar O_2 and OH airglow, Master's thesis, The Geophysical Institute, the University of Alaska Fairbanks.

Walterscheid, R. L., Sivjee, G. G. & Roble, R. G. (2000), 'Mesospheric and lower thermospheric manifestations of a stratospheric warming event over Eureka, Canada (80°N)', *Geophys. Res. Lett.* **27**(18), 2897–2900.

Whiteway, J. A. & Duck, T. J. (1996), 'Evidence for critical level filtering of atmospheric gravity waves', *Geophys. Res. Lett.* **23**(2), 145–148.

Wurtele, M. G., Sharman, R. D. & Datta, A. (1996), 'Atmospheric lee waves', *Annu. Rev. Fluid. Mech.* **28**, 429–476.

Appendix A: Presentations and publications

Before and during my thesis work I have made three presentations at various conferences and been first author on two articles. These presentations and publications are listed below.

Presentations

- "An Airborne Spectroscopy Campaign over Svalbard", poster presentation at the 1999 CEDAR[1] meeting in Boulder, Colorado.
- "An Observation of a Mesospheric Planetary Wave over Svalbard in relation to a Major Stratospheric Warming", poster presentation at the 25^{th} EGS[2] general assembly in Nice, France.
- "An Observation of a Mesospheric Planetary Wave over Svalbard in relation to a Major Stratospheric Warming", oral presentation at the year 2000 IAGA[3] workshop "Lower Atmosphere Effects on the Ionosphere and Upper Atmosphere" in Prague, Czech Republic.

Publications

- "Polar OH-airglow Temperature Variations in the 87/88 Winter", accepted for publication in Physics and Chemistry of the Earth (Nielsen et al. 2001).
- "Simultaneous Measurements of Temperatures in the Upper Mesosphere with an Ebert-Fastie Spectrometer and a VHF Meteor RADAR on Svalbard (78°N, 16°E)", accepted for publication in Geophysical Research Letters (Nielsen, Röttger & Sigernes 2001).

[1] Couplings Energetics and Dynamics in Atmospheric Research
[2] The European Geophysical Society
[3] The International Association of Geomagnetism and Aeronomy

Appendix B: Visualization of the results

```
%%%%%%%%%%%%%%%%%%%%%%%%%%%%%%%%%%%%%%%%%%%%%%%%%%%%
%%                                                 %
%% This is the main program Allread.m that         %
%% generates plots from the SyntheticOH log-files  %
%% for a specified time interval. The plots are of %
%% the original 1-hour averaged data, the data     %
%% when filtered with a 24 hour filter and the     %
%% difference between these.                       %
%% Also a plot of the distribution of the data,    %
%% with respect to time of day, can be made. In    %
%% the program the error-level desired can be set. %
%%                                                 %
%% The output arrays from the program are divided  %
%% into two groups. The first contains the arrays  %
%% that are approved according to the specified    %
%% error-level and the second contains all data.   %
%%                                                 %
%% The arrays in the first group are time_arr,     %
%% all_temp, tempb, perturbations, error_arr and   %
%% pc_error_arr. Here tempb contains the filtered  %
%% temperatures and pertubations is all_temp-tempb %
%% Time_arr give the time in different formats     %
%% according to what is desired.                   %
%%                                                 %
%% The arrays in the second group are the_lot_time %
%% the_lot_temp, tempc, the_lot_perturbations,     %
%% the_lot_error_arr and the_lot_pc_error_arr.     %
%%                                                 %
%% Kristian Pagh Nielsen, the 11th of August 2000. %
%%                                                 %
%% Latest update: the 28th of August 2000.         %
%%                                                 %
%%%%%%%%%%%%%%%%%%%%%%%%%%%%%%%%%%%%%%%%%%%%%%%%%%%%

% INPUT PARAMETERS:

all_time=zeros(6,1000);
all_error=zeros(1,1000);
```

```
all_pc_error=zeros(1,1000);
all_temp=zeros(1,1000);
all_nr=1;
the_lot_time=zeros(6,1000);
the_lot_pc_error=zeros(1,1000);
the_lot_error=zeros(1,1000);
the_lot_temp=zeros(1,1000);
the_lot_nr=1;
time_switch=2;
%NOTE time_switch=1 is day from 1980, where 'day 1' is 1/1/80!
%     time_switch=2 is daytime in a specific year.
%     time_switch=5 is time on a specific day.
if time_switch==1;
  start_year=input('Start year: ');
  start_month=input('Start month: ');
  end_year=input('End year: ');
  end_month=input('End month: ');
end
if time_switch==2;
  year=input('Year: ');
  start_year=year;
  end_year=year;
  start_month=input('Start month: ');
  end_month=input('End month: ');
end

tic

% READING THE DATA:

for y=start_year:end_year
if y~=start_year
  begin_month=1;
else
  begin_month=start_month;
end
if y~=end_year
  stop_month=12;
else
  stop_month=end_month;
```

```
end
if 1980<y & y<=1990
for m=begin_month:stop_month
for d=1:31
  count=0;
  line='fill';
  if d<10
    day=num2str(d);
    day=strcat('0',day);
  else
    day=num2str(d);
  end
  if m<10
    month=num2str(m);
    month=strcat('0',month);
  else
    month=num2str(m);
  end
  ar=num2str(y);
  ar=ar(3:4);
  ext='.log';
  dir='../data/temperatures/log_files/';
  filename=strcat(dir,day,month,ar,ext);
  ls (filename);
  if ans(1:3)=='../'
    fid=fopen(filename);
    line=fgets(fid);
    for a=1:200
      if line(a)=='_'
        break
      end
    end
    fclose(fid);
    fid=fopen(filename);
    for b=1:1000
      line=fgets(fid);
      if line~=-1
        count=count+1;
      end
    end
```

```
fclose(fid);
fid=fopen(filename);
time_arr=zeros(6,count);
error_arr=zeros(1,count);
pc_error_arr=zeros(1,count);
temp_arr=zeros(1,count);
line_nr=0;
the_lot_time_arr=zeros(6,count);
the_lot_error_arr=zeros(1,count);
the_lot_pc_error_arr=zeros(1,count);
the_lot_temp_arr=zeros(1,count);
the_lot_line_nr=0;
for l=1:count
  line=fgets(fid);
  year=line(a-4:a-1);
  start_hour=line(a+1:a+2);
  start_min=line(a+3:a+4);
  start_sec=line(a+5:a+6);
  end_hour=line(a+8:a+9);
  end_min=line(a+10:a+11);
  end_sec=line(a+12:a+13);
  if m<10
    month=line(a-5);
    if d<10
      day=line(a-6);
    else
      day=line(a-7:a-6);
    end
  else
    month=line(a-6:a-5);
    if d<10
      day=line(a-7);
    else
      day=line(a-8:a-7);
    end
  end
  start_time=str2num(start_hour)+str2num(start_min)/60+ ...
   str2num(start_sec)/3600;
  end_time=str2num(end_hour)+str2num(end_min)/60+ ...
   str2num(end_sec)/3600;
```

```
time=(start_time+end_time)/2;
daytime=str2num(day)+time/24;
if m==11
  daytime=daytime+304;
end
if m==12
  daytime=daytime+334;
end
if m==2
  daytime=daytime+31;
end
year_daytime=datenum(y,0,daytime)-datenum(1980,0,0); ...
 %NOTE 'day 1'=1/1/80!
time_vector=[year_daytime;daytime;y;m;d;time];
sign=line(a+19);
error=str2num(line(a+20:a+24));
order_sign=line(a+37);
error_order=str2num(line(a+38:a+41));
if order_sign=='-'
  error=error*10^-error_order;
else
  error=error*10^error_order;
end
if sign=='-'
  error=-error;
end
pc_error=str2num(line(a+44:a+48))*10;
temperature=str2num(line(a+68:a+72))*100;
the_lot_line_nr=the_lot_line_nr+1;
the_lot_time_arr(:,the_lot_line_nr)=time_vector;
the_lot_error_arr(the_lot_line_nr)=error;
the_lot_pc_error_arr(the_lot_line_nr)=pc_error;
the_lot_temp_arr(the_lot_line_nr)=temperature;
if error>=0.8
  line_nr=line_nr+1;
  time_arr(:,line_nr)=time_vector;
  error_arr(line_nr)=error;
  pc_error_arr(line_nr)=pc_error;
  temp_arr(line_nr)=temperature;
end
```

```
    end
    time_arr=time_arr(:,1:line_nr);
    error_arr=error_arr(1:line_nr);
    pc_error_arr=pc_error_arr(1:line_nr);
    temp_arr=temp_arr(1:line_nr);
    the_lot_time_arr=the_lot_time_arr(:,1:the_lot_line_nr);
    the_lot_error_arr=the_lot_error_arr(1:the_lot_line_nr);
    the_lot_pc_error_arr=the_lot_pc_error_arr(1:the_lot_line_nr);
    the_lot_temp_arr=the_lot_temp_arr(1:the_lot_line_nr);
    fclose(fid);
    if line_nr>=1
      all_time(:,all_nr:(all_nr+line_nr-1))=time_arr;
      all_error(all_nr:(all_nr+line_nr-1))=error_arr;
      all_pc_error(all_nr:(all_nr+line_nr-1))=pc_error_arr;
      all_temp(all_nr:(all_nr+line_nr-1))=temp_arr;
      all_nr=all_nr+line_nr;
    end
    if the_lot_line_nr>=1
      the_lot_time(:,the_lot_nr:(the_lot_nr+the_lot_line_nr-1))= ...
       the_lot_time_arr;
      the_lot_error(the_lot_nr:(the_lot_nr+the_lot_line_nr-1))= ...
       the_lot_error_arr;
      the_lot_pc_error(the_lot_nr:(the_lot_nr+the_lot_line_nr-1))= ...
       the_lot_pc_error_arr;
      the_lot_temp(the_lot_nr:(the_lot_nr+the_lot_line_nr-1))= ...
       the_lot_temp_arr;
      the_lot_nr=the_lot_nr+the_lot_line_nr;
    end
  end
end
end
else
for m=begin_month:stop_month
for d=1:31
  count=0;
  line='fill';
  if d<10
    day=num2str(d);
    day=strcat('0',day);
  else
```

```
  day=num2str(d);
end
if m<10
  month=num2str(m);
  month=strcat('0',month);
else
  month=num2str(m);
end
ar=num2str(y);
ar=ar(3:4);
ext='.log';
dir='../data/temperatures/log_files/';
filename=strcat(dir,day,month,ar,ext);
ls (filename);
if ans(1:3)=='../'
  fid=fopen(filename);
  line=fgets(fid);
  for a=1:200
    if line(a)=='_'
      break
    end
  end
  fclose(fid);
  fid=fopen(filename);
  for b=1:1000
    line=fgets(fid);
    if line~=-1
      count=count+1;
    end
  end
  fclose(fid);
  fid=fopen(filename);
  time_arr=zeros(6,count);
  error_arr=zeros(1,count);
  pc_error_arr=zeros(1,count);
  temp_arr=zeros(1,count);
  line_nr=0;
  the_lot_time_arr=zeros(6,count);
  the_lot_error_arr=zeros(1,count);
  the_lot_pc_error_arr=zeros(1,count);
```

```
    the_lot_temp_arr=zeros(1,count);
    the_lot_line_nr=0;
%    mtemp=0;
%    mtemp_count=0;
    for l=1:count
      line=fgets(fid);
      year=line(a-4:a-1);
      start_hour=line(a+1:a+2);
      start_min=line(a+3:a+4);
      start_sec=line(a+5:a+6);
      end_hour=line(a+8:a+9);
      end_min=line(a+10:a+11);
      end_sec=line(a+12:a+13);
      if m<10
        month=line(a-5);
        if d<10
          day=line(a-6);
        else
          day=line(a-7:a-6);
        end
      else
        month=line(a-6:a-5);
        if d<10
          day=line(a-7);
        else
          day=line(a-8:a-7);
        end
      end
      start_time=str2num(start_hour)+str2num(start_min)/60+ ...
       str2num(start_sec)/3600;
      end_time=str2num(end_hour)+str2num(end_min)/60+ ...
       str2num(end_sec)/3600;
      time=(start_time+end_time)/2;
      daytime=str2num(day)+time/24;
      if m==11
        daytime=daytime+304;
      end
      if m==12
        daytime=daytime+334;
      end
```

```
      if m==2
        daytime=daytime+31;
      end
      year_daytime=datenum(y,0,daytime)-datenum(1980,0,0); ...
       %NOTE 'day 1'=1/1/80!
      time_vector=[year_daytime;daytime;y;m;d;time];
      sign=line(a+19);
      error=str2num(line(a+20:a+24));
      order_sign=line(a+37);
      error_order=str2num(line(a+38:a+41));
      if order_sign=='-'
        error=error*10^-error_order;
      else
        error=error*10^error_order;
      end
      if sign=='-'
        error=-error;
      end
      pc_error=str2num(line(a+44:a+48))*10;
      temperature=str2num(line(a+68:a+72))*100;
      the_lot_line_nr=the_lot_line_nr+1;
      the_lot_time_arr(:,the_lot_line_nr)=time_vector;
      the_lot_error_arr(the_lot_line_nr)=error;
      the_lot_pc_error_arr(the_lot_line_nr)=pc_error;
      the_lot_temp_arr(the_lot_line_nr)=temperature;
      if error>=0.8
        line_nr=line_nr+1;
        time_arr(:,line_nr)=time_vector;
        error_arr(line_nr)=error;
        pc_error_arr(line_nr)=pc_error;
        temp_arr(line_nr)=temperature;
%        if count>=6
%          mtemp=mtemp+temperature;
%          mtemp_count=mtemp_count+1;
%        end
      end
    end
%    mtemp_arr(m,d)=mtemp/mtemp_count;
    time_arr=time_arr(:,1:line_nr);
    error_arr=error_arr(1:line_nr);
```

```
    pc_error_arr=pc_error_arr(1:line_nr);
    temp_arr=temp_arr(1:line_nr);
    the_lot_time_arr=the_lot_time_arr(:,1:the_lot_line_nr);
    the_lot_error_arr=the_lot_error_arr(1:the_lot_line_nr);
    the_lot_pc_error_arr=the_lot_pc_error_arr(1:the_lot_line_nr);
    the_lot_temp_arr=the_lot_temp_arr(1:the_lot_line_nr);
    fclose(fid);
    if line_nr>=1
      all_time(:,all_nr:(all_nr+line_nr-1))=time_arr;
      all_error(all_nr:(all_nr+line_nr-1))=error_arr;
      all_pc_error(all_nr:(all_nr+line_nr-1))=pc_error_arr;
      all_temp(all_nr:(all_nr+line_nr-1))=temp_arr;
      all_nr=all_nr+line_nr;
    end
    if the_lot_line_nr>=1
      the_lot_time(:,the_lot_nr:(the_lot_nr+the_lot_line_nr-1))= ...
       the_lot_time_arr;
      the_lot_error(the_lot_nr:(the_lot_nr+the_lot_line_nr-1))= ...
       the_lot_error_arr;
      the_lot_pc_error(the_lot_nr:(the_lot_nr+the_lot_line_nr-1))= ...
       the_lot_pc_error_arr;
      the_lot_temp(the_lot_nr:(the_lot_nr+the_lot_line_nr-1))= ...
       the_lot_temp_arr;
      the_lot_nr=the_lot_nr+the_lot_line_nr;
    end
  end
end
end
end
end
all_time=all_time(:,1:all_nr-1);
all_error=all_error(1:all_nr-1);
all_pc_error=all_pc_error(1:all_nr-1);
all_temp=all_temp(1:all_nr-1);
the_lot_time=the_lot_time(:,1:the_lot_nr-1);
the_lot_error=the_lot_error(1:the_lot_nr-1);
the_lot_pc_error=the_lot_pc_error(1:the_lot_nr-1);
the_lot_temp=the_lot_temp(1:the_lot_nr-1);

% FILTERING THE DATA:
```

```
filt=24;
tempb=zeros(1,all_nr-1);
for f=1:all_nr-1
  idxmin=0;
  idxmax=0;
  tidb=all_time(2,:)*24;
  evalmin=tidb(f)-((filt-1)/2);
  evalmax=tidb(f)+((filt-1)/2);
  n=0;
  o=0;
  while idxmin==0
    n=n+1;
    idxmin=eval('pdesubix(round(tidb),round(evalmin))','0');
    evalmin=evalmin+1;
    if n>filt
      evalmin=2529;
      idxmin=2529;
    end
  end
  while idxmax==0
    o=o+1;
    idxmax=eval('pdesubix(round(tidb),round(evalmax))','0');
    evalmax=evalmax-1;
    if o>filt
      evalmax=-1;
      idxmax=-1;
    end
  end
  if idxmin<=idxmax
    ttemp=mean(all_temp(idxmin:idxmax));
    tempb(f)=ttemp;
  end
end
tempc=zeros(1,the_lot_nr-1);
for f=1:the_lot_nr-1
  idxmin=0;
  idxmax=0;
  tidc=the_lot_time(2,:)*24;
  evalmin=tidc(f)-((filt-1)/2);
```

```
  evalmax=tidc(f)+((filt-1)/2);
  n=0;
  o=0;
  while idxmin==0
    n=n+1;
    idxmin=eval('pdesubix(round(tidc),round(evalmin))','0');
    evalmin=evalmin+1;
    if n>filt
      evalmin=2529;
      idxmin=2529;
    end
  end
  while idxmax==0
    o=o+1;
    idxmax=eval('pdesubix(round(tidc),round(evalmax))','0');
    evalmax=evalmax-1;
    if o>filt
      evalmax=-1;
      idxmax=-1;
    end
  end
  if idxmin<=idxmax
    ttemp=mean(the_lot_temp(idxmin:idxmax));
    tempc(f)=ttemp;
  end
end
perturbations=all_temp-tempb;
the_lot_perturbations=the_lot_temp-tempc;

% PLOTTING THE DATA:

% PLOTTING TEMPERATURES:

if the_lot_nr>1
  figure(1)
  plot(all_time(time_switch,:),all_temp,'rd', ...
   all_time(time_switch,:),tempb,'ko')
  grid
  h=title(strcat('1 hour average temperatures, year=',year));
  axis([the_lot_time(time_switch,1) the_lot_time(time_switch, ...
```

```
   the_lot_nr-1) ...
   min(the_lot_temp) max(the_lot_temp)]);
  h=xlabel('Day number');
  h=ylabel('Temperature');
  figure(2)
  plot(the_lot_time(time_switch,:),tempc,'ko')
  grid
  h=title(strcat('Filtered with a 24 hour filter, year=',year));
  axis([the_lot_time(time_switch,1) the_lot_time(time_switch, ...
   the_lot_nr-1) 150 250]);
  h=xlabel('Day number');
  h=ylabel('Temperature');
  figure(3)
  plot(all_time,tempb,'ko')
  h=xlabel('Day number');
  grid
  h=title(strcat('Filtered with a 24 hour filter, year=',year));
  axis([the_lot_time(time_switch,1) ...
   the_lot_time(time_switch,the_lot_nr-1) 150 250]);
  h=xlabel('Day number');
  h=ylabel('Temperature');

% PLOTTING PERTURBATIONS:

%  figure(3)
%  plot(all_time(time_switch,:),perturbations,'rd', ...
%   the_lot_time(time_switch,:),the_lot_perturbations,'b+')
%  grid

% DAILY DISTRIBUTION OF THE TEMPERATURES:

%  days=zeros(1,all_nr-1);
%  day_test=zeros(1,all_nr-1);
%  hour_test=zeros(1,24);
%  for a=1:all_nr-1
%    days(a)=round(all_time(2,a)-0.5);
%    day_test(a)=all_time(2,a)-days(a);
%    day_test(a)=day_test(a)*24;
%  end
%  for b=1:24
```

```
%    for a=1:all_nr-1
%      if day_test(a)>b-1
%        if day_test(a)<=b
%          hour_test(b)=hour_test(b)+1;
%        end
%      end
%    end
%  end
%  figure(4)
%  bar(hour_test/(all_nr-1)*100)
%  axis([1 24 0 25]);
%  h=title('The distribution of data with respect to the time of day');
%  h=xlabel('Hour');
%  h=ylabel('Percent of measurements');
else
  error_message='No good data!'
end

t=toc;
if t>300
  t=num2str(round(toc/60));
  Elapsed_time=strcat(t,' minutes')
else
  t=num2str(round(toc));
  Elapsed_time=strcat(t,' seconds')
end
```

Appendix C: Pressure plane movie

```
%%%%%%%%%%%%%%%%%%%%%%%%%%%%%%%%%%%%%%%%%%%%%%%%%%%
%%                                                %
%% This is a main program. It generates a movie   %
%% of the data of the Stratospheric Research      %
%% Group in Berlin for a specified time           %
%% interval, height and parameter. The induvidual %
%% movie frames shows the daily mean of the       %
%% parameter with respect to latitude and         %
%% longitude. The procedures berlin.m, month_     %
%% converter.m, date_converter.m and zeroadd.m    %
%% are used in the program.                       %
%%                                                %
%% Kristian Pagh Nielsen, the 21st of June 2000.  %
%%                                                %
%% Latest update: the 15th of September 2000.     %
%%                                                %
%%%%%%%%%%%%%%%%%%%%%%%%%%%%%%%%%%%%%%%%%%%%%%%%%%%%

global latitude longitude parameters wind_latitude ...
 wind_longitude x_winds y_winds winds number_month ...
 str_month number_day str_day x xday

% INPUT PARAMETERS:

variable=input('Parameter ("height", "temp" or "wind"): ');
if variable(1)=='w'
  meter='height';
else
  meter=variable;
end
height=input('Height in hPa (50, 30 or 10): ');
if height==50
  height_subscript=1;
end
if height==30
  height_subscript=2;
end
if height==10
```

```
  height_subscript=3;
end
str_height=num2str(height);
altitude=[50,30,10];
full_year=input('Year: ');
full_year=num2str(full_year);
year=full_year(3:4);
number_month=input('Month: ');
start_month=number_month;
end_month=number_month;
start_day=input('Start day: ');
end_day=input('End day: ');
m_count=0;

tic

% IF THE 10 hPa LEVEL IS MISSING:

if height==10
  path(strcat('../data/5x5/',meter,'_10/y',year,'/m',year,month),path)
  p=strcat('../data/5x5/',meter,'_10/y',year,'/m',year,month,'/');
  x=number_month;
  zeroadd
  month=xday;
  x=start_day;
  zeroadd
  day=xday;
  filename=strcat('d',year,month,day,'.dat');
  ls(strcat(p,filename));
  if ans(1:6)=='../dat'
    ten_level=boolean(1);
    upper_level=3;
    upper_pressure=10;
  else
    ten_level=boolean(0);
    upper_level=2;
    upper_pressure=30;
  end
  rmpath(strcat('../data/5x5/',meter,'_10/y',year,'/m',year,month))
end
```

```
% COUNTING LOOP:

for mon=start_month:end_month
  x=mon;
  zeroadd
  month=xday;
  path(strcat('../data/5x5/',meter,'_',str_height,'/y',year,'/m', ...
   year, month),path)
  p=strcat('../data/5x5/',meter,'_',str_height,'/y',year,'/m', ...
   year,month,'/');
  for d=start_day:end_day
    x=d;
    zeroadd
    day=xday;
    filename=strcat('d',year,month,day,'.dat');
    ls (strcat(p,filename));
    if ans(1:6)=='../dat'
      m_count=m_count+1;
    end
  end
  rmpath(strcat('../data/5x5/',meter,'_',str_height,'/y',year, ...
   '/m',year,month))
end

% READING AND PLOTTING THE DATA:

m1=moviein(m_count);
if variable(1)=='w'
  m2=moviein(m_count);
  m3=moviein(m_count);
end
m_count=0;
for mon=start_month:end_month
  number_month=mon;
  month_converter
  for d=start_day:end_day
    number_day=d;
    date_converter
    x=d;
```

```
zeroadd
day=xday;
filename=strcat('d',year,month,day,'.dat');
path(strcat('../data/5x5/',meter,'_',str_height,'/y',year, ...
 '/m',year, month),path)
p=strcat('../data/5x5/',meter,'_',str_height,'/y',year,'/m', ...
 year,month,'/');
ls (strcat(p,filename));
if ans(1:6)=='../dat'
  berlin;
  m_count=m_count+1;
  if variable(1)=='w'
    figure(1)
    contourf(wind_longitude,wind_latitude,x_winds,10);
    title(strcat('Zonal winds at ',str_height,' hPa',str_day, ...
     str_month,year));
    xlabel('Latitude');
    ylabel('Longitude');
    axis([5 350 40 85]);
    colorbar;
    m1(:,m_count)=getframe;
    figure(2)
    contourf(wind_longitude,wind_latitude,y_winds,10);
    title(strcat('Meridional winds at ',str_height,' hPa ', ...
     str_day, str_month,year));
    xlabel('Latitude');
    ylabel('Longitude');
    axis([5 350 40 85]);
    colorbar;
    m2(:,m_count)=getframe;
    figure(3)
    contourf(wind_longitude,wind_latitude,winds,10);
    title(strcat('Winds at ',str_height,' hPa',str_day, ...
     str_month,year));
    xlabel('Latitude');
    ylabel('Longitude');
    axis([5 350 40 85]);
    colorbar;
    m3(:,m_count)=getframe;
  else
```

```
        figure(1)
        contourf(longitude,latitude,parameters,10);
        xlabel('longitude');
        ylabel('latitude');
        axis([0 355 40 90]);
        colorbar;
        title(strcat(parameter,' at',str_height,' hPa',str_day, ...
         str_month,year));
        m1(:,m_count)=getframe;
      end
    end
  end
  rmpath(strcat('../data/5x5/',meter,'_',str_height,'/y',year, ...
   '/m',year,month))
end
if height==10
  if ten_level==0
    error_message= ...
     'No data availble from this period at the 10hPa level'
  else
    figure(1)
    movie(m1)
    if variable(1)=='w'
      figure(2)
      movie(m2)
    end
  end
else
  figure(1)
  movie(m1)
  if variable(1)=='w'
    figure(2)
    movie(m2)
    figure(3)
    movie(m3)
  end
end

t=toc;
if t>1200
```

```
  t=num2str(round(toc/60));
  Elapsed_time=strcat(t,' minutes')
else
  t=num2str(round(toc));
  Elapsed_time=strcat(t,' seconds')
end
```

Appendix D: Latitude plane movie

```
%%%%%%%%%%%%%%%%%%%%%%%%%%%%%%%%%%%%%%%%%%%%%%%%%%%%%%
%%                                                   %
%% This is a main program. It generates a movie     %
%% of the data of the Stratospheric Research        %
%% Group in Berlin for a specified time interval    %
%% and parameter of a specified latitude            %
%% plane. The induvidual movie frames shows the     %
%% daily mean of the parameter with respect to      %
%% longitude and height. The procedures berlin.m,   %
%% month_converter.m, date_converter.m and          %
%% zeroadd.m are used in the program.               %
%%                                                   %
%% Kristian Pagh Nielsen, the 10th of August 2000. %
%%                                                   %
%%%%%%%%%%%%%%%%%%%%%%%%%%%%%%%%%%%%%%%%%%%%%%%%%%%%%%

global latitude longitude parameters wind_latitude ...
 wind_longitude x_winds y_winds number_month str_month ...
 number_day str_day x xday

% INPUT PARAMETERS:

variable=input('Parameter ("height", "temp" or "wind"): ');
latitude_plane=input('Latitude: ');
latitude_plane_str=num2str(latitude_plane);
if variable(1)=='w'
  meter='height';
  latitude_index=latitude_plane/5;
  l_index_low=round(latitude_index-1/2);
  l_index_rest=latitude_index-l_index_low;
else
  meter=variable;
  latitude_index=latitude_plane/5+1;
  l_index_low=round(latitude_index-1/2);
  l_index_rest=latitude_index-l_index_low;
end
altitude=[50,30,10];
full_year=input('Year: ');
```

```
full_year=num2str(full_year);
year=full_year(3:4);
number_month=input('Month: ');
start_month=number_month;
end_month=number_month;
start_day=input('Start day: ');
end_day=input('End day: ');
m_count=0;

tic

% IF THE 10 hPa LEVEL IS MISSING:

x=start_month;
zeroadd
month=xday;
path(strcat('../data/5x5/',meter,'_10/y',year,'/m',year,month),path)
p=strcat('../data/5x5/',meter,'_10/y',year,'/m',year,month,'/');
x=start_day;
zeroadd
day=xday;
filename=strcat('d',year,month,day,'.dat');
ls(strcat(p,filename));
if ans(1:6)=='../dat'
  ten_level=boolean(1);
  upper_level=3;
  upper_pressure=10;
else
  ten_level=boolean(0);
  upper_level=2;
  upper_pressure=30;
end
rmpath(strcat('../data/5x5/',meter,'_10/y',year,'/m',year,month))

% COUNTING LOOP:

for mon=start_month:end_month
  x=mon;
  zeroadd
  month=xday;
```

```
  path(strcat('../data/5x5/',meter,'_30/y',year,'/m',year,month),path)
  p=strcat('../data/5x5/',meter,'_30/y',year,'/m',year,month,'/');
  for d=start_day:end_day
    x=d;
    zeroadd
    day=xday;
    filename=strcat('d',year,month,day,'.dat');
    ls (strcat(p,filename));
    if ans(1:6)=='../dat'
      m_count=m_count+1;
    end
  end
  rmpath(strcat('../data/5x5/',meter,'_30/y',year,'/m',year,month))
end

% READING AND PLOTTING THE DATA:

if variable(1)=='w'
  wlp_longitude=zeros(70,upper_level);
  wlp_pressure_level=zeros(70,upper_level);
  for a=1:70
    wlp_pressure_level(a,:)=altitude(1:upper_level);
  end
  lp_x_winds=zeros(70,upper_level);
  lp_y_winds=zeros(70,upper_level);
else
  lp_longitude=zeros(72,upper_level);
  lp_pressure_level=zeros(72,upper_level);
  for a=1:72
    lp_pressure_level(a,:)=altitude(1:upper_level);
  end
  lp_parameters=zeros(72,upper_level);
end
m1=moviein(m_count);
if variable(1)=='w'
  m2=moviein(m_count);
end
m_count=0;
for mon=start_month:end_month
  x=mon;
```

```
zeroadd
month=xday;
number_month=mon;
month_converter
for d=start_day:end_day
  number_day=d;
  date_converter
  x=d;
  zeroadd
  day=xday;
  filename=strcat('d',year,month,day,'.dat');
  m_count=m_count+1;
  for level=1:upper_level
    height=altitude(level);
    str_height=num2str(height);
    path(strcat('../data/5x5/',meter,'_',str_height,'/y',year, ...
     '/m',year,month),path)
    p=strcat('../data/5x5/',meter,'_',str_height,'/y',year, ...
     '/m',year,month,'/');
    ls (strcat(p,filename));
    if ans(1:6)=='../dat'
      berlin;
      if variable(1)=='w'
        if 1<=latitude_index & latitude_index<17
          wlp_longitude(:,level)=rot90(rot90(rot90 ...
           ((longitude(1,2:71))));
          lp_x_winds(:,level)=rot90(rot90(rot90 ...
           (x_winds(l_index_low,:)+l_index_rest* ...
           (x_winds(l_index_low+1,:)-x_winds(l_index_low,:)))));
          lp_y_winds(:,level)=rot90(rot90(rot90 ...
           (y_winds(l_index_low,:)+l_index_rest* ...
           (y_winds(l_index_low+1,:)-y_winds(l_index_low,:)))));
        end
      else
        if 1<=latitude_index & latitude_index<19
          lp_longitude(:,level)=rot90(rot90(rot90 ...
           ((longitude(1,1:72))));
          lp_parameters(:,level)=rot90(rot90(rot90(parameters ...
           (l_index_low,:)+l_index_rest*(parameters ...
           (l_index_low+1,:)-parameters(l_index_low,:)))));
```

```
      end
    end
  end
  rmpath(strcat('../data/5x5/',meter,'_',str_height,'/y', ...
   year,'/m',year,month))
end
if variable(1)=='w'
  if 1<=latitude_index & latitude_index<17
    figure(1)
    contourf(wlp_longitude,wlp_pressure_level,lp_x_winds,15);
    title(strcat('Zonal winds at ',latitude_plane_str,' N ', ...
     str_day,str_month,year));
    xlabel('Longitude');
    ylabel('Pressure level');
    axis([5 350 upper_pressure 50]);
    colorbar;
    m1(:,m_count)=getframe;
    figure(2)
    contourf(wlp_longitude,wlp_pressure_level,lp_y_winds,15);
    title(strcat('Meridional winds at ',latitude_plane_str, ...
     ' N ',str_day,str_month,year));
    xlabel('Longitude');
    ylabel('Pressure level');
    axis([5 350 upper_pressure 50]);
    colorbar;
    m2(:,m_count)=getframe;
  end
else
  if 1<=latitude_index & latitude_index<19
    figure(1)
    contourf(lp_longitude,lp_pressure_level,lp_parameters,15);
    xlabel('Longitude');
    ylabel('Pressure level');
    axis([0 355 upper_pressure 50]);
    colorbar;
    title(strcat(parameter,' at ',latitude_plane_str,' N ', ...
     str_day,str_month,year));
    m1(:,m_count)=getframe;
  end
end
```

```
  end
end
if 1<=latitude_index & latitude_index<19
  figure(1)
  movie(m1)
  if variable(1)=='w'
    if 1<=latitude_index & latitude_index<17
      figure(2)
      movie(m2)
    else
      Error_message='No winds can be calculated at this latitude'
    end
  end
else
  Error_message='No data at this latitude'
end

t=toc;
if t>1200
  t=num2str(round(toc/60));
  Elapsed_time=strcat(t,' minutes')
else
  t=num2str(round(toc));
  Elapsed_time=strcat(t,' seconds')
end
```

Appendix E: Zonal means over time

```
%%%%%%%%%%%%%%%%%%%%%%%%%%%%%%%%%%%%%%%%%%%%%%%%%%%
%%                                                %
%% This is a main program. It generates a figure  %
%% of the data of the Stratospheric Research      %
%% Group in Berlin for a specified time           %
%% interval, height and parameter. The figure     %
%% shows the daily means of the parameter with    %
%% respect to time and pressure. The procedures   %
%% berlin.m, month_converter.m, date_converter.m  %
%% and zeroadd.m are used in the program.         %
%%                                                %
%% Kristian Pagh Nielsen, the 21st of June 2000.  %
%%                                                %
%% Latest update: the 19th of September 2000.     %
%%                                                %
%%%%%%%%%%%%%%%%%%%%%%%%%%%%%%%%%%%%%%%%%%%%%%%%%%%%

global latitude zonal_means u_zonal_means v_zonal_means ...
 uv_zonal_means number_month str_month number_day str_day x xday

% INPUT PARAMETERS:

variable=input('Parameter ("height", "temp" or "wind"): ');
if variable(1)=='w'
  meter='height';
else
  meter=variable;
end
height=input('Height in hPa (50, 30 or 10): ');
if height==50
  height_subscript=1;
end
if height==30
  height_subscript=2;
end
if height==10
  height_subscript=3;
end
```

```
height=num2str(height);
altitude=[50,30,10];
full_year=input('Year: ');
full_year=num2str(full_year);
year=full_year(3:4);
number_month=input('Month: ');
start_month=number_month;
end_month=number_month;
start_day=input('Start day: ');
end_day=input('End day: ');
m_count=0;

tic

% IF THE 10 hPa LEVEL IS MISSING:

x=number_month;
zeroadd
month=xday;
path(strcat('../data/5x5/',meter,'_10/y',year,'/m',year, ...
 month),path)
p=strcat('../data/5x5/',meter,'_10/y',year,'/m',year, ...
 month,'/');
x=start_day;
zeroadd
day=xday;
filename=strcat('d',year,month,day,'.dat');
ls(strcat(p,filename));
if ans(1:6)=='../dat'
  ten_level=boolean(1);
  upper_level=3;
  upper_pressure=10;
else
  ten_level=boolean(0);
  upper_level=2;
  upper_pressure=30;
end
rmpath(strcat('../data/5x5/',meter,'_10/y',year,'/m',year, ...
 month))
```

```
% COUNTING LOOP:

for level=1:upper_level
  height=num2str(altitude(level));
  for mon=start_month:end_month
    x=mon;
    zeroadd
    month=xday;
    path(strcat('../data/5x5/',meter,'_',height,'/y',year,'/m', ...
     year,month),path)
    p=strcat('../data/5x5/',meter,'_',height,'/y',year,'/m', ...
     year,month,'/');
    for d=start_day:end_day
      x=d;
      zeroadd
      day=xday;
      filename=strcat('d',year,month,day,'.dat');
      ls (strcat(p,filename));
      if ans(1:6)=='../dat'
        m_count=m_count+1;
      end
    end
    rmpath(strcat('../data/5x5/',meter,'_',height,'/y',year,'/m', ...
     year,month))
  end
end

% READING THE DATA:

time_arr=zeros(19,m_count/upper_level);
latitude_arr=zeros(19,m_count/upper_level);
zonal_mean_arr=zeros(19,m_count/upper_level);
wind_time_arr=zeros(17,m_count/upper_level);
wind_latitude_arr=zeros(17,m_count/upper_level);
u_zonal_mean_arr=zeros(17,m_count/upper_level);
v_zonal_mean_arr=zeros(17,m_count/upper_level);
uv_zonal_mean_arr=zeros(17,m_count/upper_level);
m_count=0;
for mon=start_month:end_month
  number_month=mon;
```

```
  month_converter
  for d=start_day:end_day
    number_day=d;
    date_converter
    x=d;
    zeroadd
    day=xday;
    filename=strcat('d',year,month,day,'.dat');
    for level=1:upper_level
      if level==height_subscript
        height=num2str(altitude(level));
        path(strcat('../data/5x5/',meter,'_',height,'/y',year,'/m', ...
         year,month),path)
        p=strcat('../data/5x5/',meter,'_',height,'/y',year,'/m', ...
         year,month,'/');
        ls (strcat(p,filename));
        if ans(1:6)=='../dat'
          berlin;
          m_count=m_count+1;
          if variable(1)=='w'
            wind_time_arr(:,m_count)=d;
            wind_latitude_arr(:,m_count)=wind_latitude(:,1);
            u_zonal_mean_arr(:,m_count)=u_zonal_means;
            v_zonal_mean_arr(:,m_count)=v_zonal_means;
            uv_zonal_mean_arr(:,m_count)=uv_zonal_means;
          else
            latitude_arr(:,m_count)=latitude(:,1);
            time_arr(:,m_count)=d;
            zonal_mean_arr(:,m_count)=zonal_means;
          end
        end
        rmpath(strcat('../data/5x5/',meter,'_',height,'/y',year, ...
         '/m',year,month))
      end
    end
  end
end

%PLOTTING THE DATA:
```

```
if variable(1)=='w'
  if m_count>1
    figure(1)
    contourf(wind_time_arr,wind_latitude_arr,u_zonal_mean_arr,10);
    xlabel(strcat('Day in ',str_month,year));
    ylabel('Latitude');
    axis([start_day end_day 40 85]);
    colorbar;
    title(strcat('Zonal mean zonal ',lower(variable),' at ', ...
     height,' hPa'));
    figure(2)
    contourf(wind_time_arr,wind_latitude_arr,v_zonal_mean_arr,10);
    xlabel(strcat('Day in ',str_month,year));
    ylabel('Latitude');
    axis([start_day end_day 40 85]);
    colorbar;
    title(strcat('Zonal mean meridional ',lower(variable),' at ', ...
     height,' hPa'));
    figure(3)
    contourf(wind_time_arr,wind_latitude_arr,uv_zonal_mean_arr,10);
    xlabel(strcat('Day in ',str_month,year));
    ylabel('Latitude');
    axis([start_day end_day 40 85]);
    colorbar;
    title(strcat('Zonal mean ',lower(variable),' at ', ...
     height,' hPa'));
  else
    error_message='No good data!'
  end
else
  if m_count>1
    figure(1)
    contourf(time_arr,latitude_arr,zonal_mean_arr,10);
    xlabel(strcat('Day in ',str_month,year));
    ylabel('Latitude');
    axis([start_day end_day 40 90]);
    colorbar;
    title(strcat('Zonal mean',lower(parameter),' at ',height,' hPa'));
    figure(2)
    plot(time_arr(19,:),zonal_mean_arr(19,:));
```

```
    xlabel(strcat('Day in ',str_month,year));
    title(strcat(parameter,' at 90N at ',height,' hPa'));
  else
    error_message='No good data!'
  end
end

t=toc;
if t>1200
  t=num2str(round(toc/60));
  Elapsed_time=strcat(t,' minutes')
else
  t=num2str(round(toc));
  Elapsed_time=strcat(t,' seconds')
end
```

Appendix F: Zonal means 78N over time

```
%%%%%%%%%%%%%%%%%%%%%%%%%%%%%%%%%%%%%%%%%%%%%%%%%%%
%%                                                %
%% This is a main program. It generates a figure  %
%% of the data of the Stratospheric Research      %
%% Group in Berlin for a specified time           %
%% interval and parameter. The figure shows the   %
%% daily means of the zonal means of the          %
%% parameter with respect to time and pressure.   %
%% The procedures berlin.m, month_converter.m,    %
%% date_converter.m and zeroadd.m are used in the %
%% program.                                       %
%%                                                %
%% Kristian Pagh Nielsen, the 21st of June 2000.  %
%%                                                %
%% Latest update: the 19th of September 2000.     %
%%                                                %
%%%%%%%%%%%%%%%%%%%%%%%%%%%%%%%%%%%%%%%%%%%%%%%%%%%%%

global zonal_means u_zonal_means v_zonal_means number_month ...
 str_month number_day str_day x xday

% INPUT PARAMETERS

variable=input('Parameter ("height", "temp" or "wind"): ');
if variable(1)=='w'
  meter='height';
else
  meter=variable;
end
altitude=[50,30,10];
full_year=input('Year: ');
full_year=num2str(full_year);
year=full_year(3:4);
number_month=input('Month: ');
start_month=number_month;
end_month=number_month;
month=num2str(number_month);
start_day=input('Start day: ');
```

```
end_day=input('End day: ');
m_count=0;

tic

% IF THE 10 hPa LEVEL IS MISSING:

x=number_month;
zeroadd
month=xday;
path(strcat('../data/5x5/',meter,'_10/y',year,'/m',year,month),path)
p=strcat('../data/5x5/',meter,'_10/y',year,'/m',year,month,'/');
x=start_day;
zeroadd
day=xday;
filename=strcat('d',year,month,day,'.dat');
ls(strcat(p,filename));
if ans(1:6)=='../dat'
  ten_level=boolean(1);
  upper_level=3;
  upper_pressure=10;
else
  ten_level=boolean(0);
  upper_level=2;
  upper_pressure=30;
end
rmpath(strcat('../data/5x5/',meter,'_10/y',year,'/m',year,month))

% COUNTING LOOP:

for level=1:upper_level
  height=num2str(altitude(level));
  for mon=start_month:end_month
    x=mon;
    zeroadd
    month=xday;
    path(strcat('../data/5x5/',meter,'_',height,'/y',year,'/m', ...
     year,month),path)
    p=strcat('../data/5x5/',meter,'_',height,'/y',year,'/m',year, ...
     month,'/');
```

```
    for d=start_day:end_day
      x=d;
      zeroadd
      day=xday;
      filename=strcat('d',year,month,day,'.dat');
      ls (strcat(p,filename));
      if ans(1:6)=='../dat'
        m_count=m_count+1;
      end
    end
    rmpath(strcat('../data/5x5/',meter,'_',height,'/y',year,'/m', ...
     year,month))
  end
end

% READING THE DATA:

time_arr_78=zeros(3,m_count/upper_level);
pressure_arr_78=zeros(3,m_count/upper_level);
zonal_mean_arr_78=zeros(3,m_count/upper_level);
if variable(1)=='w'
  u_zonal_mean_arr_78=zeros(3,m_count/upper_level);
  v_zonal_mean_arr_78=zeros(3,m_count/upper_level);
end
h_count=0;
for mon=start_month:end_month
  number_month=mon;
  month_converter
  for d=start_day:end_day
    number_day=d;
    date_converter
    h_count=h_count+1;
    x=d;
    zeroadd
    day=xday;
    filename=strcat('d',year,month,day,'.dat');
    for level=1:upper_level
      height=num2str(altitude(level));
      path(strcat('../data/5x5/',meter,'_',height,'/y',year,'/m', ...
       year,month),path)
```

```
      p=strcat('../data/5x5/',meter,'_',height,'/y',year,'/m',year, ...
       month,'/');
      ls (strcat(p,filename));
      if ans(1:6)=='../dat'
        berlin;
        time_arr_78(:,h_count)=d;
        pressure_arr_78(:,h_count)=altitude(:);
        if variable(1)=='w'
          u_zonal_mean_78=u_zonal_means(15)+3/5* ...
           (u_zonal_means(16)-u_zonal_means(15));
          u_zonal_mean_arr_78(level,h_count)=u_zonal_mean_78;
          v_zonal_mean_78=v_zonal_means(15)+3/5* ...
           (v_zonal_means(16)-v_zonal_means(15));
          v_zonal_mean_arr_78(level,h_count)=v_zonal_mean_78;
        else
          zonal_mean_78=zonal_means(16)+3/5*(zonal_means(17)- ...
           zonal_means(16));
          zonal_mean_arr_78(level,h_count)=zonal_mean_78;
        end
      end
      rmpath(strcat('../data/5x5/',meter,'_',height,'/y',year, ...
       '/m',year,month))
    end
  end
end

%PLOTTING THE DATA:

if h_count>1
  if variable(1)=='w'
    figure(1)
    contourf(time_arr_78,pressure_arr_78,u_zonal_mean_arr_78,10);
    xlabel(strcat('Day in ',str_month,year));
    ylabel('Pressure level');
    axis([start_day end_day upper_pressure 50]);
    colorbar;
    title(strcat('Zonal mean zonal wind at 78N'));
    figure(2)
    contourf(time_arr_78,pressure_arr_78,v_zonal_mean_arr_78,10);
    xlabel(strcat('Day in ',str_month,year));
```

```
    ylabel('Pressure level');
    axis([start_day end_day upper_pressure 50]);
    colorbar;
    title(strcat('Zonal mean meridional wind at 78N'));
    figure(3)
    plot(time_arr_78(2,:),u_zonal_mean_arr_78(2,:));
    title(strcat('Zonal mean zonal wind at 78N and 30hPa'))
    xlabel(strcat('Day in ',str_month,year));
    figure(4)
    plot(time_arr_78(2,:),v_zonal_mean_arr_78(2,:));
    xlabel(strcat('Day in ',str_month,year));
    title(strcat('Zonal mean meridional wind at 78N and 30hPa'))
  else
    figure(1)
    contourf(time_arr_78,pressure_arr_78,zonal_mean_arr_78,10);
    xlabel(strcat('Day in ',str_month,year));
    ylabel('Pressure level');
    axis([start_day end_day 30 50]);
    colorbar;
    title(strcat('Zonal mean ',lower(variable),' at 78N'));
    figure(2)
    plot(time_arr_78(2,:),zonal_mean_arr_78(2,:));
    title(strcat('Zonal mean ',lower(variable),' at 78N and 30hPa'))
    xlabel(strcat('Day in ',str_month,year));
  end
else
  error_message='No good data!'
end

t=toc;
if t>300
  t=num2str(round(toc/60));
  Elapsed_time=strcat(t,' minutes')
else
  t=num2str(round(toc));
  Elapsed_time=strcat(t,' seconds')
end
```

Appendix G: Zonal mean movie

```
%%%%%%%%%%%%%%%%%%%%%%%%%%%%%%%%%%%%%%%%%%%%%%%%%%%
%%                                                %
%% This is a main program. It generates a movie   %
%% of the data of the Stratospheric Research      %
%% Group in Berlin for a specified time           %
%% interval and parameter. The induvidual movie   %
%% frames shows the daily mean of the zonal mean  %
%% of the parameter with respect to latitude and  %
%% pressure. The procedures berlin.m, month_      %
%% converter.m, date_converter.m and zeroadd.m    %
%% are used in the program.                       %
%%                                                %
%% Kristian Pagh Nielsen, the 21st of June 2000.  %
%%                                                %
%% Latest update: the 10th of August 2000.        %
%%                                                %
%%%%%%%%%%%%%%%%%%%%%%%%%%%%%%%%%%%%%%%%%%%%%%%%%%%%

global latitude zonal_means u_zonal_means v_zonal_means ...
number_month str_month number_day str_day x xday

% INPUT PARAMETERS:

variable=input('Parameter ("height", "temp" or "wind"): ');
%variable='wind';
if variable(1)=='w'
  meter='height';
else
  meter=variable;
end
altitude=[50,30,10];
full_year=input('Year: ');
%year='87';
full_year=num2str(full_year);
year=full_year(3:4);
number_month=input('Month: ');
start_month=number_month;
%start_month=input('Start month: ');
```

```
%start_month=12;
end_month=number_month;
%end_month=input('End month: ');
%end_month=12;
start_day=input('Start day: ');
%start_day=8;
end_day=input('End day: ');
%end_day=12;
m_count=0;

tic

% IF THE 10 hPa LEVEL IS MISSING:

x=number_month;
zeroadd
month=xday;
path(strcat('../data/5x5/',meter,'_10/y',year,'/m',year,month),path)
p=strcat('../data/5x5/',meter,'_10/y',year,'/m',year,month,'/');
x=start_day;
zeroadd
day=xday;
filename=strcat('d',year,month,day,'.dat');
ls(strcat(p,filename));
if ans(1:6)=='../dat'
  ten_level=boolean(1);
  upper_level=3;
  upper_pressure=10;
else
  ten_level=boolean(0);
  upper_level=2;
  upper_pressure=30;
end
rmpath(strcat('../data/5x5/',meter,'_10/y',year,'/m',year,month))

% COUNTING LOOP:

for level=1:upper_level
  height=num2str(altitude(level));
  for mon=start_month:end_month
```

```
    x=mon;
    zeroadd
    month=xday;
    path(strcat('../data/5x5/',meter,'_',height,'/y',year,'/m', ...
     year,month),path)
    p=strcat('../data/5x5/',meter,'_',height,'/y',year,'/m',year, ...
     month,'/');
    for d=start_day:end_day
      x=d;
      zeroadd
      day=xday;
      filename=strcat('d',year,month,day,'.dat');
      ls (strcat(p,filename));
      if ans(1:6)=='../dat'
        m_count=m_count+1;
      end
    end
    rmpath(strcat('../data/5x5/',meter,'_',height,'/y',year,'/m', ...
     year,month))
  end
end

% READING AND PLOTTING THE DATA:

h_latitude=zeros(19,upper_level);
h_pressure_level=zeros(19,upper_level);
for a=1:19
  h_pressure_level(a,:)=altitude(1:upper_level);
end
h_zonal_means=zeros(19,upper_level);
wh_latitude=zeros(17,upper_level);
wh_pressure_level=h_pressure_level(2:18,:);
h_u_zonal_means=zeros(17,upper_level);
h_v_zonal_means=zeros(17,upper_level);
m1=moviein(m_count/upper_level);
if variable(1)=='w'
  m2=moviein(m_count/upper_level);
end
h_count=0;
for mon=start_month:end_month
```

```
number_month=mon;
month_converter
for d=start_day:end_day
  number_day=d;
  date_converter
  h_count=h_count+1;
  x=d;
  zeroadd
  day=xday;
  filename=strcat('d',year,month,day,'.dat');
  for level=1:upper_level
    height=num2str(altitude(level));
    path(strcat('../data/5x5/',meter,'_',height,'/y',year,'/m', ...
     year,month),path)
    p=strcat('../data/5x5/',meter,'_',height,'/y',year,'/m', ...
     year,month,'/');
    ls (strcat(p,filename));
    if ans(1:6)=='../dat'
      berlin
      if variable(1)=='w'
        wh_latitude(:,level)=latitude(2:18,1);
        h_u_zonal_means(:,level)=u_zonal_means(:,1);
        h_v_zonal_means(:,level)=v_zonal_means(:,1);
      else
        h_latitude(:,level)=latitude(:,1);
        h_zonal_means(:,level)=zonal_means(:,1);
      end
    end
    rmpath(strcat('../data/5x5/',meter,'_',height,'/y',year, ...
     '/m',year,month))
  end
  if variable(1)=='w'
    figure(1)
    contourf(wh_latitude,wh_pressure_level,h_u_zonal_means,10);
    xlabel('latitude');
    ylabel('Pressure level');
    axis([40 85 upper_pressure 50]);
    colorbar;
    title(strcat('Zonal ',variable,str_day,str_month,year));
    m1(:,h_count)=getframe;
```

```
      figure(2)
      contourf(wh_latitude,wh_pressure_level,h_v_zonal_means,10);
      xlabel('latitude');
      ylabel('Pressure level');
      axis([40 85 upper_pressure 50]);
      colorbar;
      title(strcat('Meridional ',variable,str_day,str_month,year));
      m2(:,h_count)=getframe;
    else
      figure(1)
      contourf(h_latitude,h_pressure_level,h_zonal_means,10);
      xlabel('latitude');
      ylabel('Pressure level');
      axis([40 90 upper_pressure 50]);
      colorbar;
      title(strcat(parameter,' ',str_day,str_month,year));
      m1(:,h_count)=getframe;
    end
  end
end
figure(1)
movie(m1)
if variable(1)=='w'
  figure(2)
  movie(m2)
end

t=toc;
if t>1200
  t=num2str(round(toc/60));
  Elapsed_time=strcat(t,' minutes')
else
  t=num2str(round(toc));
  Elapsed_time=strcat(t,' seconds')
end
```

Appendix H: Subroutines for reading the Berlin data

```
%%%%%%%%%%%%%%%%%%%%%%%%%%%%%%%%%%%%%%%%%%%%%%%%%%%
%%                                                %
%% This is the procedure berlin.m. It cannot be   %
%% run by itself! It reads the position           %
%% and a chosen parameter of the Berlin data for  %
%% a specific day. Also zonal means of the        %
%% parameter are calculated. The input variable   %
%% is the string: filename and the output         %
%% variables are the double arrays: latitude,     %
%% longitude, wind_latitude, wind_latitude, wind_ %
%% longitude, parameters, x_winds, y_winds,       %
%% winds, zonal_means, u_zonal_means, v_zonal_    %
%% means and uv_zonal_means.                      %
%%                                                %
%% Kristian Pagh Nielsen, the 22nd of May 2000.   %
%%                                                %
%% Latest update: The 15th of September 2000.     %
%%                                                %
%%%%%%%%%%%%%%%%%%%%%%%%%%%%%%%%%%%%%%%%%%%%%%%%%%%

global latitude longitude parameters zonal_means wind_latitude
wind_longitude x_winds y_winds winds u_zonal_means v_zonal_means
uv_zonal_means

fid=fopen(filename);
line=fgets(fid);
numline=str2num(line);
pressure=numline(1);
index_1=numline(2);
if index_1==1
  parameter='Geopotential height';
else
  parameter='Temperature';
end
index_2=numline(3);
if index_2==0
  time_average='Day';
else
```

```
  time_average='Month';
end
two_digit_year=numline(4);
latitude=zeros(19,72);
longitude=zeros(19,72);
for a=1:72
  longitude(:,a)=a*5-5;
end
parameters=zeros(19,72);
zonal_means=zeros(19,1);
for a=1:18
  for b=1:8
    line=fgets(fid);
    numline=str2num(line);
    parameters(a,b*9-8:b*9)=numline;
  end
  zonal_temp=parameters(a,:);
  zonal_means(a)=mean(zonal_temp);
  latitude(a,:)=a*5-5;
end
line=fgets(fid);
numline=str2num(line);
latitude(19,:)=90;
parameters(19,:)=numline;
zonal_means(19,1)=mean(parameters(19,:));
fclose(fid);
if length(parameter)==11
  parameters=parameters/10;
  zonal_means=zonal_means/10;
end
if length(parameter)==19
  parameters=parameters/1000;
  zonal_means=zonal_means/1000;
  if variable(1)=='w'
    geopotentials=parameters*9.807*1000;
    earth_rotation=7.292e-5;
    wind_latitude=latitude(2:18,2:71);
    wind_longitude=longitude(2:18,2:71);
    x_winds=zeros(17,70);
    y_winds=zeros(17,70);
```

```
    winds=zeros(17,70);
    u_zonal_means=zeros(17,1);
    v_zonal_means=zeros(17,1);
    for lat=2:18
      for lon=2:71
        x_winds(lat-1,lon-1)=-(geopotentials(lat+1,lon)- ...
         geopotentials(lat-1,lon))/2/earth_rotation/ ...
         sin(latitude(lat,lon)/360*2*pi)/(111111+1/9)/ ...
         (latitude(lat+1,lon)-latitude(lat-1,lon));
        y_winds(lat-1,lon-1)=(geopotentials(lat,lon+1)- ...
         geopotentials(lat,lon-1))/2/earth_rotation/ ...
         sin(latitude(lat,lon)/360*2*pi)/(111111+1/9)/ ...
         cos(latitude(lat,lon)/360*2*pi)/(longitude(lat,lon+1)- ...
         longitude(lat,lon-1));
        winds(lat-1,lon-1)=sqrt(x_winds(lat-1,lon-1)^2+ ...
         y_winds(lat-1,lon-1)^2);
      end
      u_zonal_temp=x_winds(lat-1,:);
      u_zonal_means(lat-1,:)=mean(u_zonal_temp);
      v_zonal_temp=y_winds(lat-1,:);
      v_zonal_means(lat-1,:)=mean(v_zonal_temp);
      uv_zonal_temp=winds(lat-1,:);
      uv_zonal_means(lat-1,:)=mean(uv_zonal_temp);
    end
  end
end
```

```
%%%%%%%%%%%%%%%%%%%%%%%%%%%%%%%%%%%%%%%%%%%%%%%%%%%
%%                                                %
%% This is the procedure zeroadd.m. It adds 0 to  %
%% variables that are less than ten. It can be    %
%% used when reading filenames. It uses input     %
%% variable x (a number) and the output variable  %
%% is xday (a string).                            %
%%                                                %
%% Kristian Pagh Nielsen, the 22nd of May 2000.   %
%%                                                %
%%%%%%%%%%%%%%%%%%%%%%%%%%%%%%%%%%%%%%%%%%%%%%%%%%%

global x xday
if x<10
  xday=num2str(x);
  xday=strcat('0',xday);
else
  xday=num2str(x);
end
```

```
%%%%%%%%%%%%%%%%%%%%%%%%%%%%%%%%%%%%%%%%%%%%%%%%%%%
%%                                                %
%% This is the procedure date_converter.m. It     %
%% converts days from numbers to their respective %
%% names. It uses input variable number_day       %
%% (a number between 1 and 31) and the            %
%% output variable is str_day.                    %
%%                                                %
%% Kristian Pagh Nielsen, the 31st of May 2000.   %
%%                                                %
%%%%%%%%%%%%%%%%%%%%%%%%%%%%%%%%%%%%%%%%%%%%%%%%%%%

global number_day str_day
day_ext_arr=['st';'nd';'rd';'th';'th';'th';'th';'th';'th';'th'; ...
 'th';'th';'th';'th';'th';'th';'th';'th';'th';'th';'st';'nd'; ...
 'rd';'th';'th';'th';'th';'th';'th';'th';'st'];
day_ext=day_ext_arr(number_day,:);
number_day=num2str(number_day);
number_day=strcat(' ',number_day);
str_day=strcat(' the',number_day,day_ext,' of');
```

```
%%%%%%%%%%%%%%%%%%%%%%%%%%%%%%%%%%%%%%%%%%%%%%%%%%%
%%                                                %
%% This is the procedure month_converter.m.       %
%% It is used to convert months from numbers to   %
%% their respective names. It uses input variable %
%% number_month (a number between 1 and 12) and   %
%% the output variable is str_month.              %
%%                                                %
%% Kristian Pagh Nielsen, the 31st of May 2000.   %
%%                                                %
%%%%%%%%%%%%%%%%%%%%%%%%%%%%%%%%%%%%%%%%%%%%%%%%%%%

global number_month str_month
str_month_arr=['   January';'  February';'     March'; ...
 '     April';'       May';'      June';'      July';'    August'; ...
 ' September';'   October';'  November';'  December'];
str_month=str_month_arr(number_month,:);
```